This manuscript has been published in Biointerphases. 2015 Dec 19;10(4):041004. doi: 10.1116/1.4933243.

Title: On modeling and nano-analysis of caries-affected dentin surfaces restored with Zn-containing amalgam and *in vitro* oral function.

Short title: Analysis of load cycled carious dentin, treated with amalgams.

Authors: Manuel Toledano[1*], Fátima S. Aguilera[1], Estrella Osorio[1], Modesto T.López-López[2], Inmaculada Cabello[1], Manuel Toledano-Osorio[1], Raquel Osorio[1].

Institution: [1]University of Granada, Faculty of Dentistry, Dental Materials Section.

Address: [1]University of Granada, Faculty of Dentistry, Dental Materials Section
Colegio Máximo de Cartuja s/n
18071 – Granada - Spain.
[2] University of Granada, Faculty of Science, Applied Physics Department
Fuente Nueva s/n
18071 – Granada - Spain.

*Corresponding author: Prof. Manuel Toledano
University of Granada, Faculty of Dentistry
Dental Materials Section
Colegio Máximo de Cartuja s/n
18071 – Granada - Spain.
Tel.: +34-958243788
Fax: +34-958240809
Email: toledano@ugr.es

ABSTRACT

The aim of this research was to assess the influence of mechanical loading on the ability of Zn-free *vs* Zn-containing amalgams to promote remineralization at the dentin interface. Sound (SD) and caries-affected dentin surfaces (CAD) were restored using Zn-free or Zn-containing dental amalgams. Mid-coronal dentin surfaces were studied by 1) Atomic Force Microscopy (AFM) analysis (including plot and phase imaging, nano-indentation test (modulus of Young (E_i), nano-roughness measurements, and fibril diameter assessment), 2) Raman spectroscopy/cluster analysis, 3) X-ray diffraction (μXRD^2), 4) field emission electron microscope (FESEM) and energy-dispersive analysis (EDX), for morphological, mechanical, and physico-chemical characterization. Analyses were performed before amalgam placement and after amalgam removal, at 24 hours and 3 weeks of load cycling. Zn-free and Zn-containing amalgams restorations promoted an increase in the modulus of Young of CAD surfaces, after three weeks of load cycling; at this time, Zn-containing amalgams attained higher E_i than Zn-free restorations. Zn-containing amalgams induced tubular occlusion after load cycling, in both sound and CAD. Zn free-amalgams promoted remineralization of both intertubular and peritubular dentin in CAD substrata. These minerals were identified as calcium-phosphate deposits, and crystals as hydroxyl-apatite with augmented crystallographic maturity but with some components of lattice distortion. Crosslinking of collagen diminished and secondary structure of collagen increased in CAD substrate restored with Zn-containing amalgam after 3 w of load cycling, indicating an advanced preservation, molecular organization and orientation of collagen fibrils after load cycling. Plot and phase images permitted to observe the topographical changes which were promoted by the mineral deposits; in general, the indexes related to higher remineralization gave rise to a decrease of nano-roughness and an augmentation of the

bandwidth of the collagen fibrils. Zn-containing amalgam restorations submitted to mechanical stimuli promote remineralization of the partially mineral-depleted subjacent substrate at the caries-affected dentin.

Key words: load cycling, dentin, amalgam, zinc, remineralization, caries, demineralization.

I. INTRODUCTION

Sound dentin is a hydrated (23% vol.) structure, composed of a mineral phase in the form of needle- and plate-shaped biological calcium-deficient, carbon-rich apatite crystallites (48% vol.). The main structural component of dentin are type I collagen fibrils and a minor presence of other proteins (29% vol.) impregnated and surrounded by mineral crystallites, which have c-axes aligned with the collagen fibrils axis[1]. Dentin demonstrates hierarchical structure at the nano- and micro-scales with organic and inorganic components organized in substructures optimized by evolution to withstand environmental stresses associated with their biological function[2]. Nevertheless, non carious or sound dentin (SD) is not the substrate most frequently involved in clinical dentistry. Instead, dentists usually must place restorative materials on irregular dentin substrates such as carious dentin[3]. Caries-affected dentin (CAD) is partially demineralized and more porous than noncarious dentin with a predominantly intact collagen matrix, whose collagen fibrils retain their banded structure and intermolecular crosslinks[4]. It should be preserved during clinical treatment because it is remineralizable and serves as a suitable substrate for tooth repair[5] and physiologic remineralization[6]. According to a survey carried out in USA, amalgam continues to play a major role in restorative dentistry, today[7], though it is not an ideal material, as the cosmetic appearance is poor and cannot bond to tooth[8].

Dental amalgam, a dental restorative filling material alloy that consists of approximately 50% mercury, was introduced in clinical dentistry over 150 years ago and has provided a valuable and relatively inexpensive service for patients ever since. Currently, it is an effective restorative material; its popularity arising from its ease of use, good long-term performance, safe to use, and low cost[8]. At the present time, there is no conclusive evidence suggesting risk of adverse systemic effects. Amalgam is being

discontinued in response to global concerns about mercury in the environment, but the evidence brought by studies assessing the environmental risks is based on estimations and assumptions; therefore, no concrete conclusions can be drawn[9]. In addition, mercury exposure from dental amalgam has decreased significantly in recent years due to the responsible professional conduct and proper mercury hygiene protocols [9]. The Food and Drug Administration (FDA) and the American Dental Association (ADA) support amalgam as safe and effective material for dental restorations[10,11]. The FDA also claims that the levels of exposure from amalgams are well below levels actually known to cause adverse effects, and notes that amalgam is a commonly used device with a low frequency of adverse events reported to the agency [12]. Moreover, results from the only two randomized, controlled, clinical trials on dental amalgams found no difference in neurobehavioral outcomes between the amalgam group and the composite (non-amalgam) group[13], providing evidence for the safety of amalgam[11,12]. The majority of the studies which do not recommend the clinical use of dental amalgams handle insufficient time-frames as well as flawed measures of exposure such as blood or urine levels, and none appear to consider genetic susceptibilities [14]. Resin composite is the most common alternative to dental amalgam, but possesses inherent clinical disadvantages compared to amalgam including reduced wear resistance, compressive strength, fracture resistance, coupled with increase microleakage, marginal staining and secondary caries. The clinical procedure is also more time-consuming and technique sensitive[15-17].

Alloys containing more than 0.01 wt% zinc are identified as Zn-containing amalgams; those containing less than 0.01 wt% of zinc are known as Zn-free amalgams[18]. Zn-containing amalgams enhanced the physical, mechanical and electro-chemical properties of the restoration, and it also increases the heterogeneity and so, the

fatigue resistance of the amalgam microstructure[19]. Zn-rich products at the tooth-amalgam interface, as $ZnSn(OH)^6$, ZnO_2, and Zn^{++} free [20], improved the sealing of the dentin-amalgam interface, enhancing the clinical lifetime of this restoration [21]. Previous outcomes have demonstrated that Zn-containing amalgams promoted an increase of nanomechanical properties, and a general augmentation of mineral gradients, ratios and crystallinity in partially mineral-depleted dentin surfaces. Therefore, specific Zn-containing amalgams do have therapeutic and protective effects for inducing mineral precipitations within the partially demineralized caries affected dentin-amalgam interface. Moreover, corrosion products at the interface and further uptake of metal ions associated or not to Zn might have performed as nuclei for apatite precipitation at the collagen fibers [22]. Nevertheless, the clinical significance of these results might be questioned as they were not performed with oral function.

In the oral environment, teeth are subjected to challenges provided by mechanical stresses from mastication and para-functional habits. Mechanical cycling has been widely used as potential aging methods that, additionally, stimulates challenges *in vitro*, *i.e.*, dentin remineralization [23]. Remineralization is the process of delivery of mineral (calcium and phosphate), from outside the tooth into previously demineralized hard tissue. Remineralization of CAD has, as its ultimate goal, the re-establishment of the functionality of the affected tissue, which can be described as the competence of the dentin in accomplishing its role in the tooth. Simple precipitation of mineral into the loose demineralized dentin matrix may be of relatively high mineral content but with low mechanical properties, misleading information on the actual effectiveness of the remineralization approaches[24]. The nanomechanical assessment permits specific evaluation of the elastic mechanical properties of dentin regions in both sound and carious tissue [25]. Spectroscopic analyses, such as Raman allow the determination of the

nature of the minerals and also provide quantitative information in mineral and matrix composition as mineralization occurs. Micro X-ray diffraction (μXRD^2) is one of the most powerful techniques to study the hierarchical structure of biological mineral composites such as teeth and bone [26]. Field emission scanning electron and atomic force microscopy may contribute, in addition, to the histo-morphological assessment at the restorative-dentin interface.

The purpose of this research was to assess the influence of mechanical loading on the ability of Zn-free *vs* Zn-containing amalgams to induce mineral formation at the dentin-amalgam interface. The null hypothesis is that, after load cycling, remineralization is not produced at the sound dentin or caries-affected dentin surfaces when Zn-free or Zn-containing amalgams are employed for restorations.

II. MATERIAL AND METHODS

A. Specimens preparation and mechanical loading

Nine extracted carious third molars without opposing occlusion were employed for the study. They were stored in 0.01% (w/v) thymol at 4º C for less than 1 month. Teeth were collected after written patients' informed consent (20 to 40 yr of age), under a protocol approved by the Institution Review Board (891/1014). Specimens were randomly assigned to two groups (n= 4) according to the type of amalgam to be used: with or without zinc. The inclusion criteria for carious dentin substrate were that the caries lesion, surrounded by sound dentin, was limited to the occlusal surface and it was extended at least half the distance from the enamel-dentin junction to the pulp chamber. To obtain caries affected dentin, grinding was performed by using the combined criteria of visual examination, surface hardness using a dental explorer, and staining by a caries detector solution (CDS, Kuraray Co., Ltd., Osaka, Japan). Using this procedure it was

removed all soft stainable, carious dentin. It was left the relatively hard, caries-affected dentin, non stainable, on the experimental side. Flat mid-coronal sound dentin, and caries affected dentin surfaces surrounded by normal dentin, were exposed using a hard tissue microtome (Accutom-50; Struers, Copenhagem, Denmark) equipped with a slow-speed, water-cooled diamond wafering saw (330-CA RS-70300, Struers, Copenhagen, Denmark).

Molars were transversally sectioned (Isomet 4000, Buehler, Lake Bluff, IL, USA) at the mid-coronal portion of each tooth, to produce dentin discs (2.5 mm thick), and were polished through SiC abrasive papers up to 4,000-grit with a final polishing procedure performed with diamond pastes (Buehler-MetaDi, Buehler Ltd.), through 1 μm down to 0.25 μm. The specimens were treated in ultrasonic bath (Model QS3, Ultrawave Ltd, Cardiff, UK) containing deionized water [pH 7.4] for 5 min at each polishing step.

Two self threading titanium retentive pins (4.4 mm length) (STP Restorative Dentsply Maillefer, Ballaigues, Switzerland) were used to retain the amalgam restorations, by using copper bands (Copper Bands, Hard. AB Dentatus, Spånga, Sweden), surrounding the prepared dentin discs. A tile of dental amalgam was condensed on top of the disc surfaces in a layer of at least 3 mm thick. Finally, the amalgam surfaces were finished with hand instruments. The detailed composition of each amalgam is shown in Table I.

Table I. Composition of amalgams used in the present study.

AMALGAM	COMPOSITION	
	Alloy powder	**Weight %**
Megalloy EZ®* (Zn-free)	Silver	56.7 %
	Tin	28.6 %
	Copper	14.7%
The recommended alloy to mercury ratio by mass is approximately 1.3:1		
Dispersalloy®* (Zn-containing)	Silver	69 %
	Tin	18 %
	Copper	12 %
	Zinc	1 %
The recommended alloy to mercury ratio by mass is approximately 1:1		

* DENTSPLY DETREY GmbH Konstanz, Germany.

Restored teeth were stored for 24 hours in simulated body fluid solution (SBFS), pH 7.45, at 37 ºC. SBFS composition comes from the revised version of the ISO standard ISO 23317:2012: NaCl 8.035 g, $NaHCO_3$ 0.355 g, KCl 0.225 g, $K_2HPO_4 \cdot 3H_2O$ 0.231 g, $MgCl_2 \cdot 6H_2O$ 0.311 g, 1.0 M – HCl 39 ml, $CaCl_2$ 0.292 g, Na_2SO_4 0.072 g, Tris 6.118 g, 1.0 M – HCl 0–5 ml. Specimens were then subjected to mechanical loading (100,000 cycles, 3 Hz, 49 N, for 9.2 h) (S-MMT-250NB; Shimadzu, Tokyo, Japan), and stored until 24 h. At his moment, specimens were divided into two halves . One half of each tooth was analyzed and the other half was submitted to load cycling (100,000 cycles, 3 Hz, 49 N) every seven days until completing a period of SBFS storage, for 3 w (four load cycles, in total), to determine the possible apatite formation at this time point [27]. To proceed with the mechanical loading, specimens were mounted in plastic rings using a dental stone. The cycling compressive load was applied to the amalgam restoration using a 5-mm diameter spherical stainless steel plunger, while immersed in SBFS. The amalgam tiles were removed from the discs by cutting away the amalgam around the retentive pins. All specimens were submitted to Atomic Force Microscopy (AFM)

analysis, RAMAN and XRD analyses before and after amalgams placement. Scanning Electron Microscopy (SEM) analysis was only performed after removal of amalgam restorations.

B. Atomic Force Microscopy (AFM) analysis

B.1. Nano-indentation test

An atomic force microscope (AFM Nanoscope V, Digital Instruments, Veeco Metrology group, Santa Barbara, CA, USA) equipped with a Triboscope indentor system (Hysitron Inc., Minneapolis, MN) was employed in this study. The process was undertaken inside a wet cell in a fully hydrated state (Digital Instrument, Santa Barbara, CA, USA). To facilitate CAD areas identification, they were marked with a diamond point. The nanoindentation process was performed using a Berkovich diamond indenter with a tip radius of 20 nm. Ten indentations with a peak of load of 4000 nN and a time function of 10 s were performed on each dentin disc. From these experiments, the nanoindentation modulus (E_i) of the samples, was obtained. This nanoindentation modulus, obtained by AFM, is usually referred to as Young's modulus in the literature, which should not be confounded with the Young's modulus obtained at the macroscopic level by traction/compression experiments.

In our nanoindentation experiments the indenter was progressively (at a constant rate) pressed over the sample up to a peak load of 4000 nM (loading part of the experiment) and, afterwards, the load was progressively released to zero value (unloading part of the experiment). From these experiments the load, *F*, was obtained as a function of the penetration depth, *h*, of the indenter in the sample. From the slope of these load-vs.-depth curves the nanoindentation modulus (Young's modulus) can be obtained by application of different theoretical models [28,29]. One of these is the Oliver-Pharr method, which is based on a continuum, isotropic, homogeneous elastic contact

model to determine the reduced modulus, E_r. In this model the slope, S, of the unloading portion of the load-vs.depth data is used to obtain E_r according to the following equation [29]:

$$S = \frac{dF}{dh} = \frac{2}{\sqrt{\pi}} E_r \sqrt{A}, \qquad (1)$$

where A is the projected contact area of the hardness impression of the indenter. Then, E_i of the sample is obtained through the following expression:

$$\frac{1}{E_r} = \frac{\left(1-\nu_{ind}^2\right)}{E_{ind}} + \frac{\left(1-\nu_i^2\right)}{E_i}, \qquad (2)$$

In this expression "*i*" subscript refers to the tested sample and "*ind*" subscript to the indenter. ν and E are the Poisson's ratio and the Young's modulus, respectively. For hard materials, as dentin, Usually, $E_{ind} >> E_i$ and, thus, the contribution of the indenter in equation (2) can be neglected.

Young's modulus values were automatically calculated (Triboscan Quasi version 8.4.2.0 Hysitron, Inc), and afterwards analyzed by two-way ANOVA and Student-Newman-Keuls multiple comparisons ($P<0.05$). Analysis of interactions was included. Differences between attained values at pre and post-amalgam conditions were analyzed by Student's t test ($P<0.01$).

B.2. Nanoroughness measurements

Three 15 μm x 15 μm digital images were recorded from each surface with a slow scan rate (0.1 Hz). The 15 μm x 15 μm images were analyzed quantitatively. For each image, five randomized boxes (1x1 μm) were created to examine the intertubular roughness of dentin. Nanoroughness (Ra, in nanometer) was measured using a proprietary software (Nanoscope Software version V7).

B.3. Fibril diameter assessment.

Collagen fibril diameter was determined from the 2x2 μm images by section analysis using data that had been modified only by plane fitting. Five fibrils were analyzed from each image. Measurements were corrected for tip broadening [30] by the equation $e=2r$, where e is the error in the horizontal dimension and r is the tip's radius [31].

As the normality assumption of the data was valid, numerical data were analyzed with ANOVA and Student-Newman-Keuls multiple comparison tests, with statistical significance preset at $\alpha=0.05$.

C. Raman spectroscopy and cluster analysis

A dispersive Raman spectrometer/microscope (Horiba Scientific Xplora, Villeneuve d´Ascq, France) was used to analyse dentin surfaces. A 785-nm diode laser (100 mW sample power) and an X100/0.90 NA air objective were employed. Raman signal was acquired using a 600-lines/mm grating centered between 200 and 1,700 cm^{-1}. Chemical mapping of the surfaces was performed and submitted to K-means cluster (KMC) analysis using the multivariate analysis tool (ISys® Horiba), which includes statistical pattern to derive the independent clusters. The K-means clustering is a method of cluster analysis based on a centroid model which aims to partition n observations into k clusters in which each observation belongs to the cluster with the nearest mean[32]. The biochemical content of each cluster was analyzed using the average cluster spectra. Principal component analysis (PCA) decomposed data set into a bilinear model of linear independent variables, the so-called principal components (PCs). For each specimen, a 12μm x 12μm area of the surface was mapped using 0.5 μm spacing at X and Y axes, at 100x magnification. A total of 625 points were performed per map. The resolution of the mapping was 6.25 cm^{-1}. Clusters were created following Ward's technique and the dendrogram was calculated applying four factor spectra or principal

components, corresponding to four different histological locations of both sound or caries affected dentin surfaces. The aim of a factor analysis lies in the effective reduction of the dataset dimension while maintaining a maximum of information. This method was used to model the data and to determine spectral variances associated for data differentiation. It resulted in the calculation of a new coordinate system whereby variations of the dataset is described via new axes, principal components (PCs). As the cluster centroids are essentially means of the cluster score for the elements of cluster, the mineral and organic components of substrata were examined for each cluster. At this point, the relative presence of mineral, crystallinity, gradient in mineral content, the phosphate peak ratio, crosslinking and nature of collagen were assessed [33].

Relative presence of mineral:

1. *Phosphate* (960 cm^{-1}) *and carbonate* (1070 cm^{-1}) *peaks and areas of their bands.* Peak heights were processed in absorbance units.
2. *Relative mineral concentration* (i.e., mineral-to-matrix ratio): It was inferred from the visible ratio of the intensities of the peaks at 960 cm^{-1} (phosphate) (PO_4^{3-}) and 1003 cm^{-1} (phenyl group), the aromatic ring of phenylalanine residues in collagen, or peaks at 1070 cm^{-1} (carbonate) (CO_3^{2-}) and 1003 cm^{-1}. These indexes concerned with the maximum relative degree of mineralization [34,35]. Additionally, peaks at 960 cm^{-1} and 1450 (CH_2) or 1070 cm^{-1} and 1450 can be used [36].

Crystallinity: It was evaluated based on the full width at half maximum (Raman-FWHM) of the phosphate band at 960 cm^{-1} and carbonate band at 1070 cm^{-1}. These indexes expressed the crystallographic or relative atomic order, since narrower peaks suggest less structural variation in bond distances and angles [34]. In general, the narrower the spectral peak width is, the higher the degree of mineral crystallinity [35].

Gradient in mineral content, or carbonate content of the mineral crystallites: It was assessed as the relationship between the ratio of heights at 1070 cm^{-1} (carbonate) (CO_3^{2-}) to 960 cm^{-1} (phosphate) (PO_4^{3-}), indicating carbonate substitution for phosphate [34].

The organic component of dentin was analyzed examining the following parameters:

Normalization: Phenyl group: The peak at 1003 cm^{-1}, which is assigned to C-C bond in the phenyl group, was used for normalization[37].

Crosslinking:

1. Pyridinium ring vibration: In the spectra, the peak appeared at 1030/1032.7 cm^{-1}, is assigned to the C-C in pyridinium ring vibration which has a trivalent amino acid crosslinking residue [38]. The relative intensity of this peak increases after the crosslinking formation [39].
2. Ratio Pyridinium/Phenyl (1031 cm^{-1}/1001 cm^{-1}): the higher the ratio, the greater the extend of collagen cross-linking [39,40].
3. Ratio 1660 (amide I)/1690-1701: decreases when mineralization increases.
4. Ratio 1003 (phenyl)/1450 (CH_2): arises preceding deposition of HAP (hydroxyapatite) crystals within the structure [36].
5. AGEs (advance glycation end products)-pentosidine at 1550 cm^{-1}, interpreted as a marker of the aging process [41].

Carboxylic group COO^-: The 1415 cm^{-1} band assigned to COO^- stretching mode is related with the formation of ionic bonds with calcium [42].

Lipids: Detection of extra-cellular lipids and phospholipids bands at 1440 and 1465 cm^{-1} reveals the presence of debris of cell membranes, and play an important role during the early stage of hard tissue healing or maturation [43].

Nature of collagen:

1. Amide III, CH and Amide I: The peaks at 1246/1270, 1450 and 1655/1667 cm^{-1}, assigned to amide III, CH and amide I, respectively, are sensitive to the molecular conformation of the polypeptide chains [37,39]. The decrease of amide I peak indicates damage or removal of collagen fibrils [40].
2. Amide II: from peptide bonds (~1560 cm−1, N-H bending, and C-N stretching) [44].
3. Ratio amide I/amide III concerned the organization of collagen.
4. Ratio amide III /CH_2 wagging mode indicates the structural differences [45].
5. Ratio amide I/CH_2 indicates altered collagen quality [45].
6. Ratio I/AGEs-Pentosidine, indicative of the glycation reaction *vs* collagen scaffolding [45].
7. 1340 cm^{-1} peak: This signal has been assigned to protein α-helices where intensity is sensitive to molecular orientation [36].

D. X-Ray Diffraction (XRD), Field Emission Scanning Electron Microscopy (FESEM) and energy dispersive (SEM/EDX) analyses

The X-ray micro-diffractometer (μXRD^2) used in this study was a single crystal diffractometer with a 2-dimensional detector system Cmos Photon 100 (Bruker-D8 Venture, Wien, Austria), equipped with kappa geometry based goniometer 2D Detector and XRD 2D Scan software. The X-ray beam (Cu Kα line, λ = 1.5418 Å) was generated by a Cu Microforms source Iμs and generator settings of 50.00 kV/1.00 mA were employed. The 2D position sensitive detector had 1024x1024 pixels. Both the starting and ending positions were: distance, 40.00 mm; 2θ: 40.00°; Omega: 20.00°; Phi: 270.00°; Chi: 50.00°. Wavelength of 1.54184 Å (Cu). The sample to detector distance was 40.00 mm, 2θ scaning angle range was from 10° to 80°. All measurements were

performed at room temperature (295±0.1°K) and an exposure time: 60.00 s were followed. A voltage of 50.00 kV, a current of 1.000 mA with the anode of Cu were used for the generator. For the detector, a frame size of 1024 pixels/ 98.30 mm, 104.17 pixels per centimeter in square shape were utilized. CuKα radiation was executed in $\theta-\theta$ scan. The tooth section was fixed to the sample holder. The XRD lines were identified by comparing the measured patterns to the JCPDS (Joint Committee on Powder Diffraction Standars) data cards (International Centre for Diffraction Data, 2005) [46].

Specimens were then fixed in a solution of 2.5% glutaraldehyde in 0.1 mol/L sodium cacodylate buffer for 24 h, rinsed three times in 0.1 mol/L sodium cacodylate buffer. Samples were placed in an apparatus for critical point drying (Leica EM CPD 300, Wien, Austria). They were then sputter-coated with carbon by means of a sputter-coating Nanotech Polaron-SEMPREP2 (Polaron Equipment Ltd., Watford, UK) and observed with a field emission scanning electron microscope (FESEM Gemini, Carl Zeiss, Oberkochen, Germany) at an accelerating voltage of 3 kV. Energy-dispersive analysis was performed in selected points using an X-ray detector system (EDX Inca 300, Oxford Instruments, Oxford, UK) attached to the FESEM.

III. RESULTS AND DISCUSSION

This study demonstrated that Zn-containing amalgams restorations submitted to three weeks of load cycling promoted intrafibrillar mineralization of the partially mineral-depleted in caries-affected dentin surfaces.

Attained Young's modulus is displayed in Table II.

Table II. Mean (SD) of Young Modulus (GPa) measured at the experimental dentin surfaces.

YOUNG´S MODULUS (E_i) (GPa)				
Amalgam		**Initial**	**24h (1 load cyclic)**	**3w (4 load cyclic)**
Megalloy EZ® (Zn-free)	Sound dentin	22.62 (1.37) a1	11.86 (3.98) b1	25.51 (2.85) a1
	CAD	2.48 (0.43) a2	0.08 (0.01) b2	16.72 (2.44) c2
Dispersalloy® (Zn-containing)	Sound dentin	20.10 (4.40) a1	20.15 (3.10) a3	17.03 (2.5) a2
	CAD	2.61 (0.50) a2	11.77 (1.68) b1	23.40 (1.67) c1

CAD: Caries-affected dentin. For each horizontal row: values with identical letters indicate no significant difference using Student t-test (P>0.01). For each vertical column: values with identical numbers indicate no significant difference using Student t-test (P>0.05).

Raman spectroscopy-cluster analysis results are shown in Tables III and IV.

Table IIIa. Mineral components in dentin surfaces treated with Zn-free amalgam.

		Relative Presence of Mineral								FWHM		GMC Ratio C/P
		Phosphate [961]				Carbonate [1070]						
		Peak	Area	RMC	MMR	Peak	Area	RMC	MMR	Phosphate	Carbonate	
Sound dentin	24h	67.95	1724.54	14.55	12.82	11.76	581.6	2.52	2.22	19.35	37.91	0.17
	3w	51.51	1524.33	13.14	13.66	8.62	391.49	2.20	2.29	22.01	34.77	0.17
CAD	24h	31.55	800.64	11.19	9.33	4.72	290.9	1.67	1.40	22.58	47.38	0.15
	3w	38.74	983.2	6.63	7.55	7.2	622.41	1.23	1.40	19.36	66.72	0.19

CAD: Caries-affected dentin; RMC: Relative Mineral Concentration between mineral/Phenyl (1003); MMR: Mineral/Matrix (CH_2) Ratio;
FWHM- Full-width half-maximum; GMC: Gradient in Mineral Content (carbonate peak/phosphate peak). Peaks positions are expressed in cm^{-1}.

Table IIIb. Organic components (normalization, crosslinking, carboxylic group and lipids) in dentin surfaces treated with Zn-free amalgam.

		Normalization	Crosslinking					Carboxilic Group COO^- [1415]	Lipids	
		Phenyl [1003]	Pyrid. [1032]	Ratio [1032/1003]	Ratio [1660/1690]	Ratio phenyl/CH_2 [1003/1450]	AGEs-Pentosidine [1550]		[1440]	[1465]
Sound dentin	24h	4.67	5.70	1.22	2.42	0.88	1.69	2.93	3.97	4.23
	3w	3.92	3.99	1.02	1.93	1.04	1.65	2.41	3.24	2.98
CAD	24h	2.82	2.63	0.93	2.71	0.83	1.43	2.16	2.80	2.90
	3w	5.84	2.67	0.46	1.10	1.14	3.18	3.79	5.05	4.53

CAD: Caries-affected dentin; Pyrid: Pyridinium; A: amide; AGEs: advanced glycation end products. Peaks positions are expressed in cm^{-1}.

Table IIIc. Organic components (nature and secondary structure of collagen) in dentin surfaces treated with Zn-free amalgam.

		A-III [1246-1270]	CH_2 [1450]	A-I [1655-1667]	A-II [1560]	Ratio A-I/ A-III	Ratio A-III/ CH_2	Ratio A-I/ CH_2	Ratio A-I/ AGEs-Pentosidine	α-helices [1340]
Sound dentin	24h	8.85	5.3	1.74	1.25	0.20	1.67	0.33	1.03	3.68
	3w	5.9	3.77	1.7	1.03	0.29	1.56	0.45	1.03	2.61
CAD	24h	5.75	3.38	1.33	0.93	0.23	1.70	0.39	0.93	3.07
	3w	7.85	5.13	5.24	2.32	0.67	1.53	1.02	1.65	5.52

CAD: Caries-affected dentin; A-III: Amide III; A-I: Amide I; A-II: Amide II; AGEs: advanced glycation end products. Peaks positions are expressed in cm^{-1}.

Table IVa. Mineral components in dentin surfaces treated with Zn-containing amalgam.

		Relative Presence of Mineral								FWHM		GMC Ratio C/P
		Phosphate [961]				Carbonate [1070]						
		Peak	Area	RMC	MMR	Peak	Area	RMC	MMR	Phosphate	Carbonate	
Sound dentin	24h	77.31	2292.33	5.57	6.26	19.85	187.9	1.43	1.61	19.40	34.84	0.26
	3w	124.3	3687.17	18.44	13.08	20.72	940.55	3.07	2.18	20.97	34.77	0.17
CAD	24h	30.74	909.58	4.22	7.28	7.54	1319.15	1.03	1.79	22.58	58.17	0.25
	3w	66.05	1675.65	6.05	11.59	13.89	1198.93	1.27	2.44	19.35	66.69	0.21

CAD: Caries-affected dentin; RMC: Relative Mineral Concentration between mineral/Phenyl (1003); MMR: Mineral/Matrix (CH_2) Ratio;
FWHM- Full-width half-maximum; GMC: Gradient in Mineral Content (carbonate peak/phosphate peak). Peaks positions are expressed in cm^{-1}.

Table IVb. Organic components (normalization, crosslinking, carboxylic group and lipids) in dentin surfaces treated with Zn-containing amalgam.

		Normalization	Crosslinking					Carboxilic Group COO^-	Lipids	
		Phenyl [1003]	Pyrid. [1032]	Ratio [1032/1003]	Ratio [1660/1690]	Ratio phenyl/CH_2 [1003/1450]	AGEs-Pentosidine [1550]	[1415]	[1440]	[1465]
Sound dentin	24h	13.89	15.84	1.14	1.19	1.12	8.3	10.54	12.35	10.54
	3w	6.74	11.86	1.76	1.86	0.71	2.89	6.24	8.71	7.73
CAD	24h	7.29	7.17	0.98	1.97	1.73	2.45	3.53	4.23	3.21
	3w	10.92	6.18	0.57	1.16	1.92	7.16	5.54	6.16	5.17

CAD: Caries-affected dentin; Pyrid: Pyridinium; A: amide; AGEs: advanced glycation end products. Peaks positions are expressed in cm^{-1}.

Table IVc. Organic components (nature and secondary structure of collagen) in dentin surfaces treated with Zn-containing amalgam.

		A-III [1246-1270]	CH_2 [1450]	A-I [1655-1667]	A-II [1560]	Ratio A-I/ A-III	Ratio A-III/ CH_2	Ratio A-I/ CH_2	Ratio A-I/ AGEs-Pentosidine	α-helices [1340]
Sound dentin	24h	12.14	12.35	12.7	2.87	1.05	0.98	1.03	1.53	11.95
	3w	21.53	9.5	4.56	1.83	0.21	2.27	0.48	1.58	8.14
CAD	24h	6.71	4.22	1.83	1.95	0.27	1.59	0.43	0.75	5.2
	3w	9.28	5.7	6.74	3.32	2.66	0.73	1.63	1.30	0.94

CAD: Caries-affected dentin; A-III: Amide III; A-I: Amide I; A-II: Amide II; AGEs: advanced glycation end products. Peaks positions are expressed in cm^{-1}.

RAMAN analysis of sound dentin after removal of load cycled Zn-free amalgam restoration is shown in Figure 1.

Figure 1

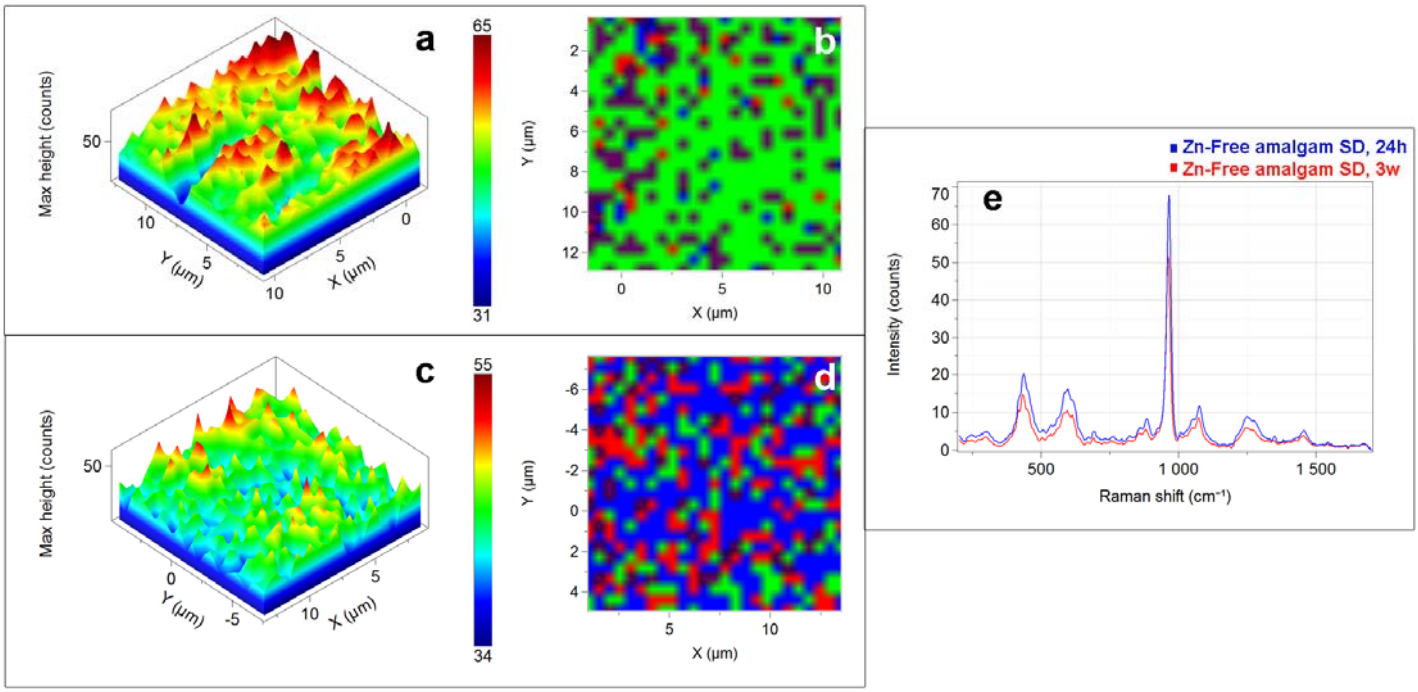

Figure 1. RAMAN analysis of sound dentin after removal of load cycled Zn-free amalgam restoration. 3D micro-Raman map of 961 cm^{-1} intensities at the dentin surface when load cycling was applied for 24 h **(a)** or 3 w **(c)**. At the 3D micro-Raman, blue represents the lowest peak intensity, while the red represents the highest. K-means clustering (KMC) map of the Raman profile of the same samples, when load cycling was applied for 24 h **(b)** or 3 w **(d)**. **(e)** Raman spectra of the principal component. SD: sound dentin.

RAMAN analysis of caries-affected dentin after removal of load cycled Zn-free amalgam restoration is shown in Figure 2.

Figure 2

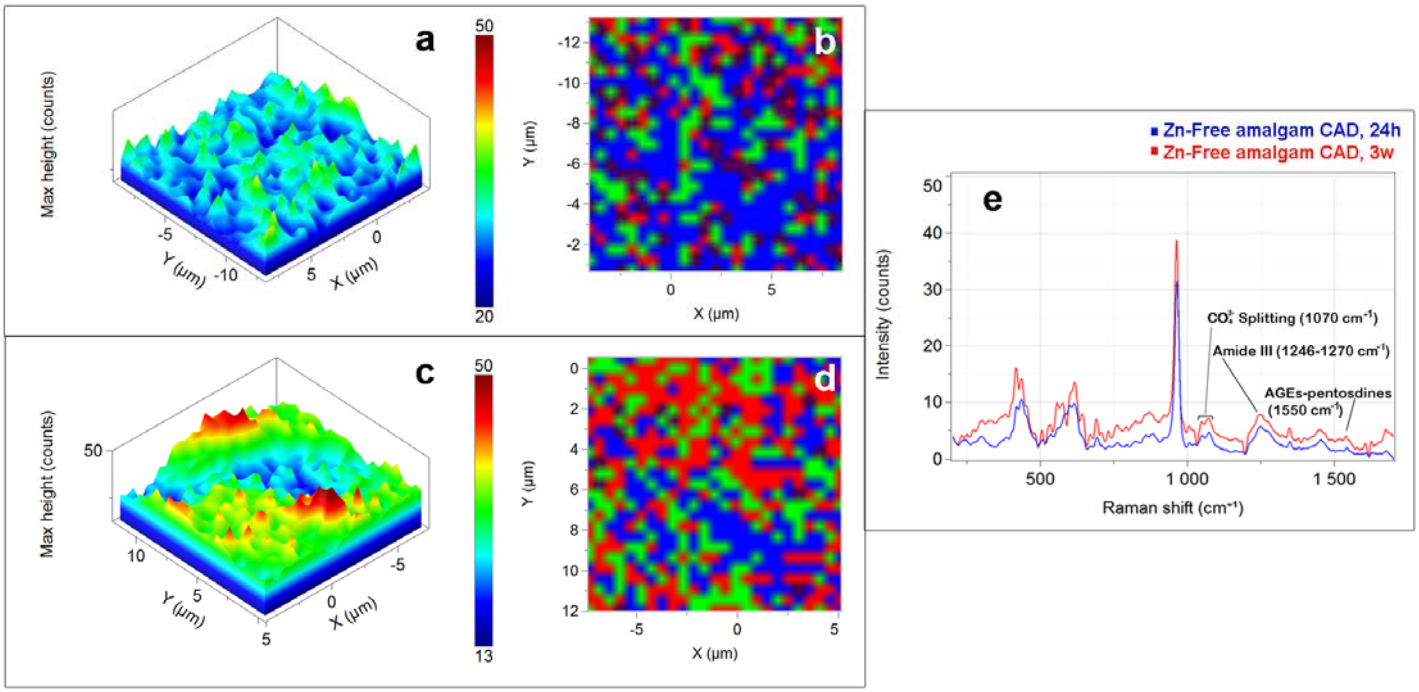

Figure 2. RAMAN analysis of caries-affected dentin after removal of load cycled Zn-free amalgam restoration. 3D micro-Raman map of 961 cm^{-1} intensities at the dentin surface when load cycling was applied for 24 h **(a)** or 3 w **(c)**. At the 3D micro-Raman, blue represents the lowest peak intensity, while the red represents the highest. K-means clustering (KMC) map of the Raman profile of the same samples, when load cycling was applied for 24 h **(b)** or 3 w **(d)**. **(e)** Raman spectra of the principal component. CAD: caries-affected dentin.

RAMAN analysis of sound dentin after removal of load cycled Zn-containing amalgam restoration is shown in Figure 3.

Figure 3

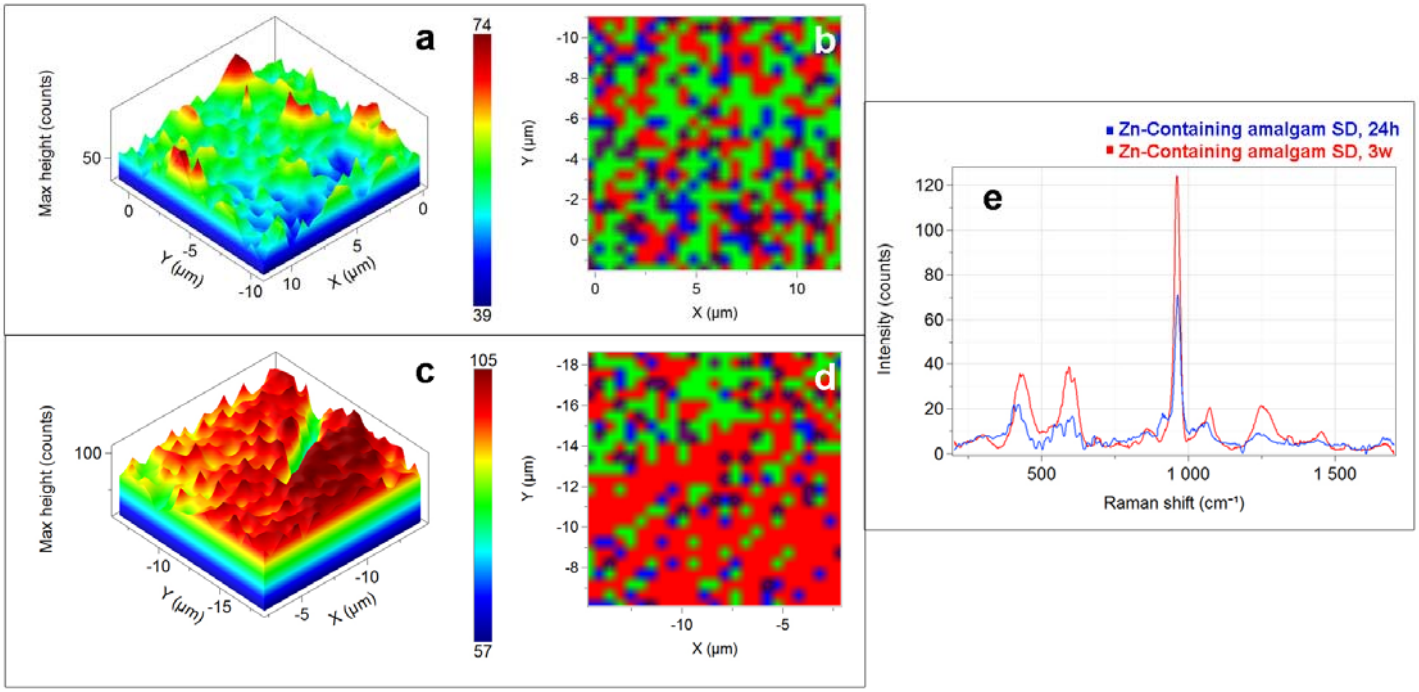

Figure 3. RAMAN analysis of sound dentin after removal of load cycled Zn-containing amalgam restoration. 3D micro-Raman map of 961 cm^{-1} intensities at the dentin surface when load cycling was applied for 24 h **(a)** or 3 w **(c)**. At the 3D micro-Raman, blue represents the lowest peak intensity, while the red represents the highest. K-means clustering (KMC) map of the Raman profile of the same samples, when load cycling was applied for 24 h **(b)** or 3 w **(d)**. **(e)** Raman spectra of the principal component. SD: sound dentin.

RAMAN analysis of caries-affected dentin after removal of load cycled Zn-containing amalgam restoration is shown in Figure 4.

Figure 4

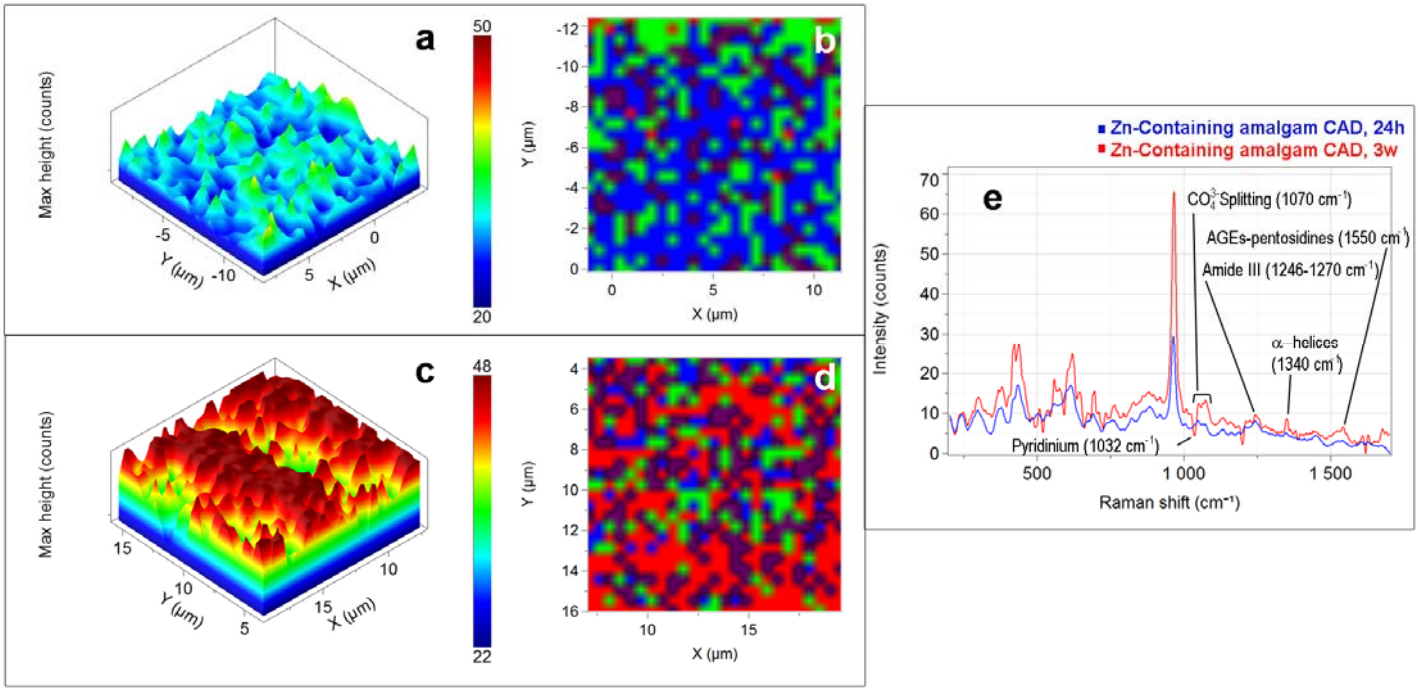

Figure 4. RAMAN analysis of caries-affected dentin after removal of load cycled Zn-containing amalgam restoration. 3D micro-Raman map of 961 cm^{-1} intensities at the dentin surface when load cycling was applied for 24 h **(a)** or 3 w **(c)**. At the 3D micro-Raman, blue represents the lowest peak intensity, while the red represents the highest. K-means clustering (KMC) map of the Raman profile of the same samples, when load cycling was applied for 24 h **(b)** or 3 w **(d)**. **(e)** Raman spectra of the principal component. CAD: caries-affected dentin.

FESEM images and EDX spectra are displayed in Figure 5.

Figure 5

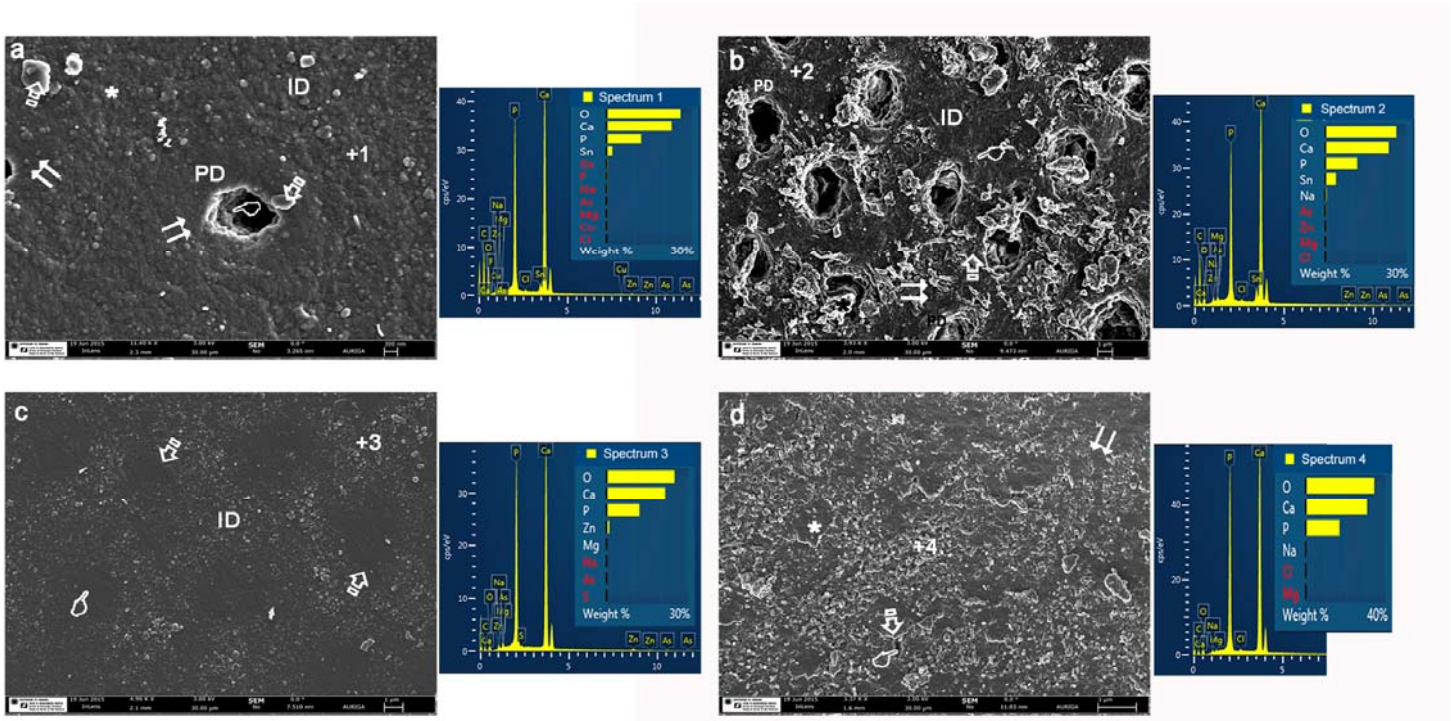

Figure 5. (a): FESEM image and EDX spectrum of caries-affected dentin after removal of Zn-free amalgam restoration, and 24 h of load cycling. Peritubular (PD) and intertubular (ID) dentin were strongly mineralized. A consistent and continuous layer of mineral was observed covering the intertubular dentin (asterisk). Mineralized collagen fibrils were not noticeable below this coat of new crystals. Some crystals or mineral deposits were occasionally encountered on both intertubular and peritubular dentin (arrows). Tubules appeared mineral free with a clear ring of peritubular dentin (double arrow) and a robust peritubular dentin wall (pointer). Ep1 is an EDX spectrum indicating presence of phosphorous (P), calcium (Ca) and tin (Sn). (**b):** FESEM image and EDX spectrum of caries-affected dentin (CAD) after removal of Zn-free amalgam restoration, and 3 w of load cycling. A compact mineralized layer appeared covering the whole intertubular dentin (ID). At peritubular dentin (PD), mineral formed a lip around each tubule lumen detected. Collagen fibers were clearly observed at peritubular dentin, some of them partially (arrow), or totally remineralized (pointer), permitting to observe the presence of mineral crystals embedded in a remnant collagen scaffold-like structure. Multiple mineralized formations scattered throughout the total surface of dentin (double arrow), but allowing the visual observation of tubule walls. Some non-sealed tubules turned up partially mineral filled (asterisk). Collagen fibrils appeared longitudinally mineralized, rounding the entrance of tubules. Ep2 is an EDX spectrum, corresponding to intertubular dentin location, indicating presence of phosphate (P), calcium (Ca) and tin (Sn), among the principal components. **(c):** FESEM image and EDX spectrum of sound dentin after removal of Zn-containing amalgam restoration, and 24 h of load cycling. Tubules appeared totally mineral-occupied with a complete hermetic sealing

(arrows). Crystals precipitated in small and inter-connected knob-like formations, at intertubular dentin (ID), and smaller at intratubular dentin (pointer). Zinc-based salts [phosphorous (P), calcium (Ca), and zinc (Zn)] were detected in the elemental analysis (EDX, spectrum 3). **(d):** FESEM image and EDX spectrum of caries-affected dentin (CAD) after removal of Zn-containing amalgam restoration and 3 w of load cycling. A consistent and continuous layer of mineral was observed covering the intertubular dentin (asterisk), precipitating in a dense network of multilayered crystals on the dentin surface. These crystal formations did not allow to see the subjacent collagen fibers, and covered partially (arrow) or totally (double arrow) the entrance of tubules. Some terminal knob-like mineral structures were exhibited on the dentin surface, occupying spaces among the mineral scales. Most of the tubules appeared mineral-occupied without hermetic sealing (pointer), in some cases. Ep4 is an EDX spectrum, corresponding to intertubular dentin location, indicating presence of phosphate (P), and calcium (Ca).

Figure 6 is showing the refined μXRD^2 profiles attained in the experimental groups.

Figure 6a

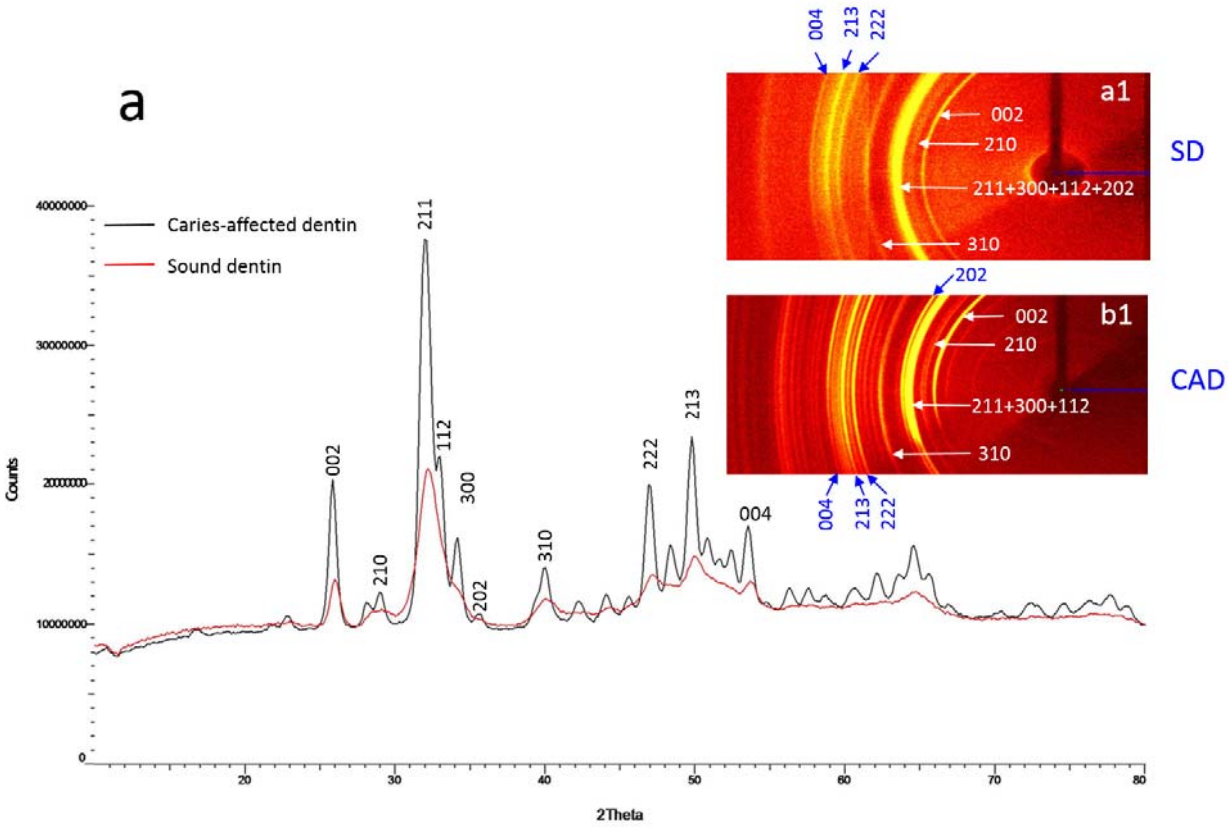

Figure 6b

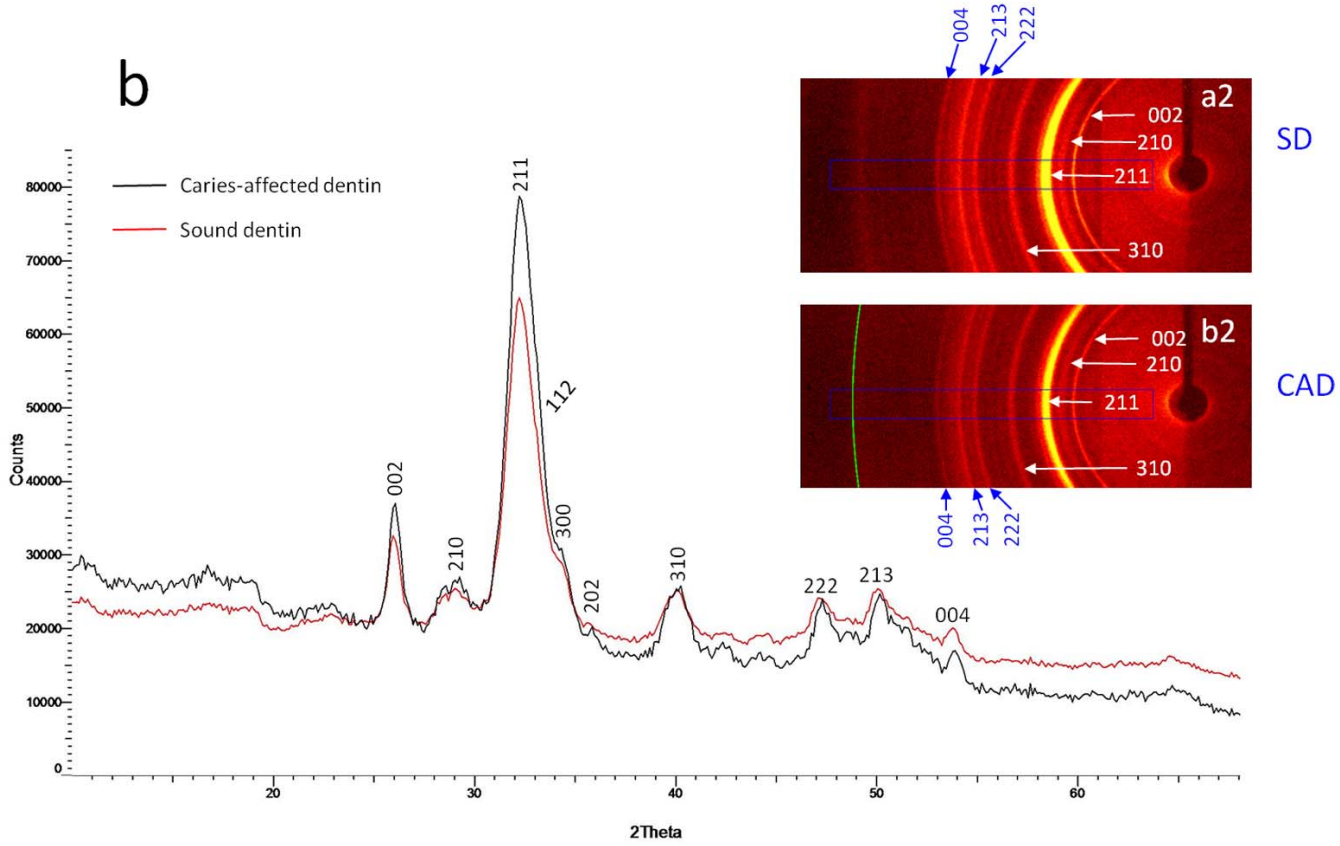

Figure 6c

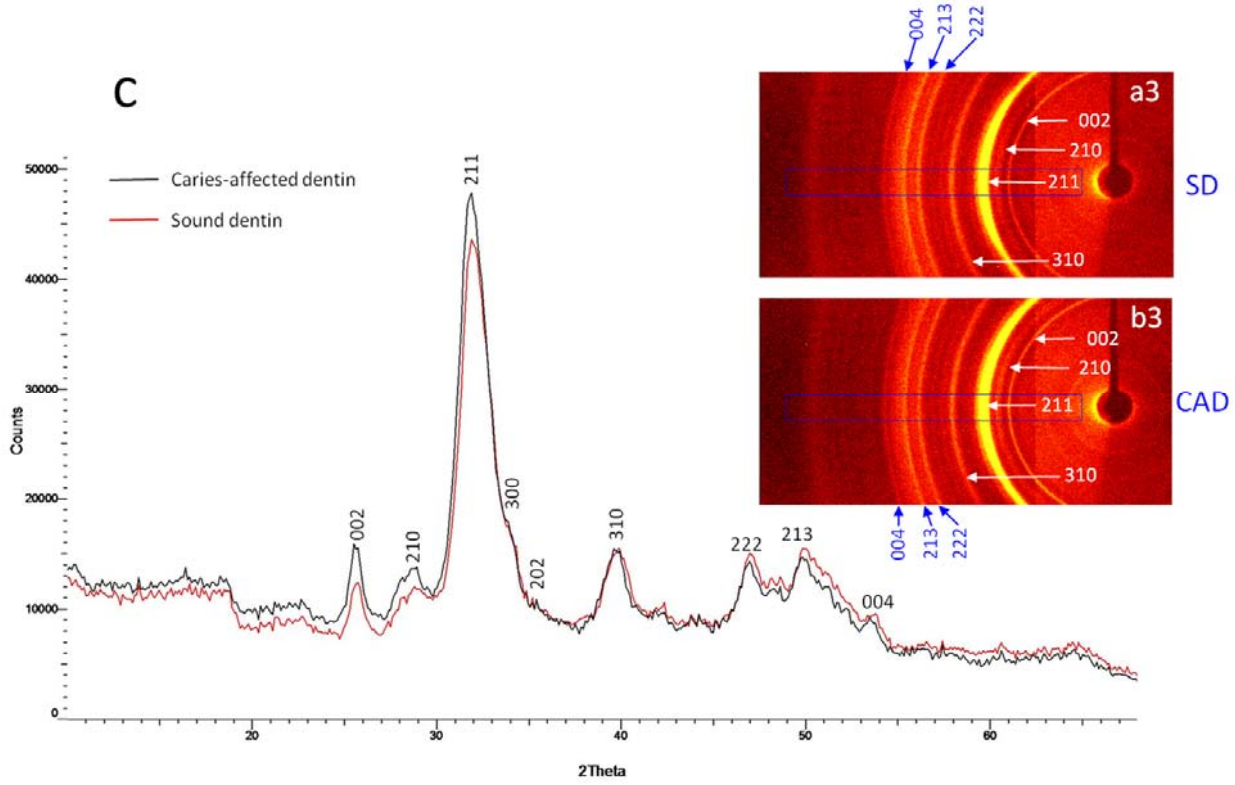

Figure 6. **(a)** Refined μXRD^2 profiles of unloaded sound and caries-affected dentin. The corresponding Debye-Scherrer rings are shown in inset a1 (sound dentin) and b1 (caries-affected dentin). **(b)** Refined μXRD^2 profiles of sound and caries-affected dentin after removal of Zn-free amalgam and three weeks of load cycling. The corresponding Debye-Scherrer rings are shown in inset a2 (sound dentin) and b2 (caries-affected dentin). **(c)** Refined μXRD^2 profiles of sound and caries-affected dentin after removal of Zn-containing amalgam and three weeks of load cycling. The corresponding Debye-Scherrer rings are shown in inset a3 (sound dentin) and b3 (caries-affected dentin).

Mean and standard deviation of nanoroughness SRa (nm) measured on sound and caries-affected dentin surfaces, after removal of Zn-free or -containing amalgam restorations, unloaded or after 24 hours or 3 weeks of load cycling, is observed in Figure 7.

Figure 7

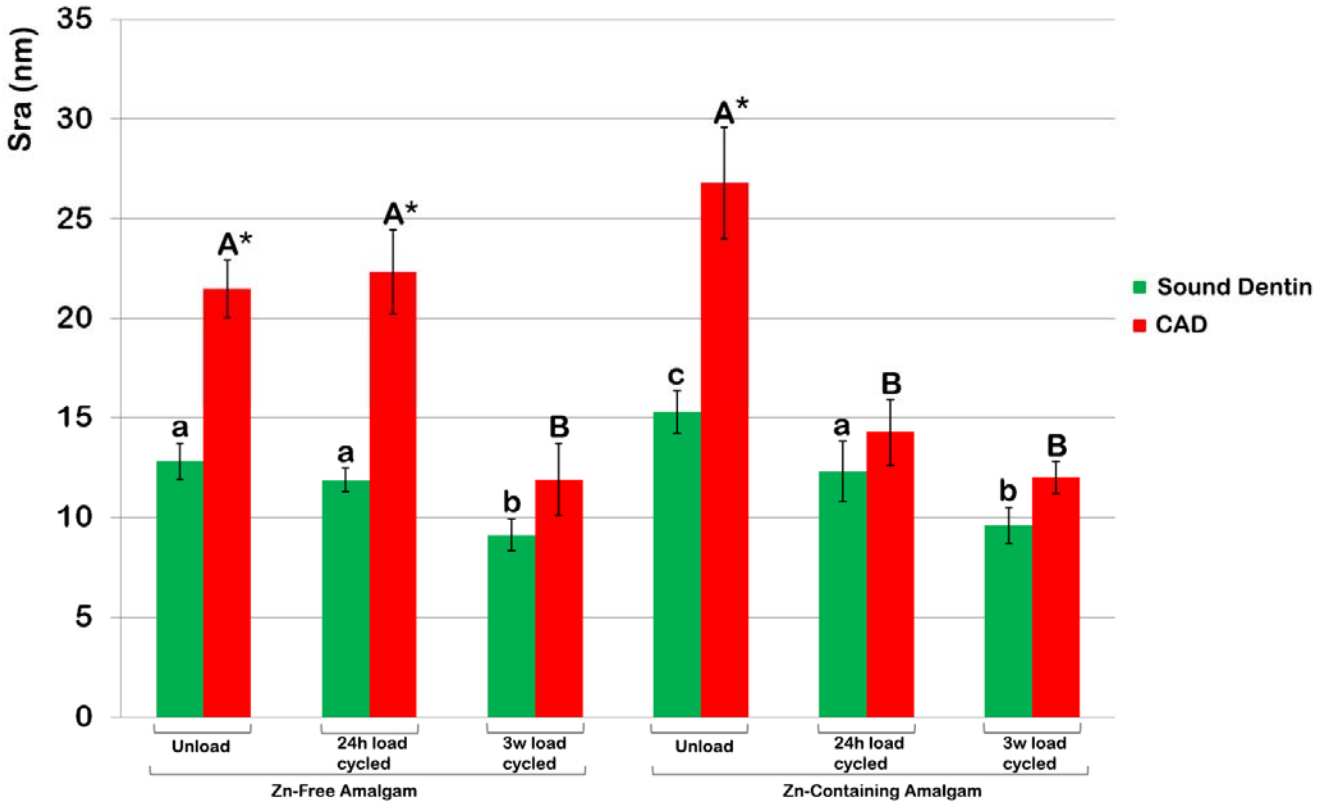

Figure 7. Mean and standard deviation of nanoroughness SRa (nm) measured on sound and caries-affected dentin surfaces, after removal of Zn-free or -containing amalgam restorations, unloaded or after 24 hours or 3 weeks of load cycling. Identical letters

(lower case, sound dentin; capital, caries-affected dentin) indicate no significant differences after Student-Newman-Keuls test ($p>0.05$). *indicates significant differences between sound dentin and caries-affected dentin, within the same loading and amalgam group.

Mean and standard deviation of fibrils width (nm) before amalgam application and after removal of Zn-free or -containing amalgam restorations, unloaded or after 24 hours or 3 weeks of load cycling, is shown in Figure 8.

Figure 8

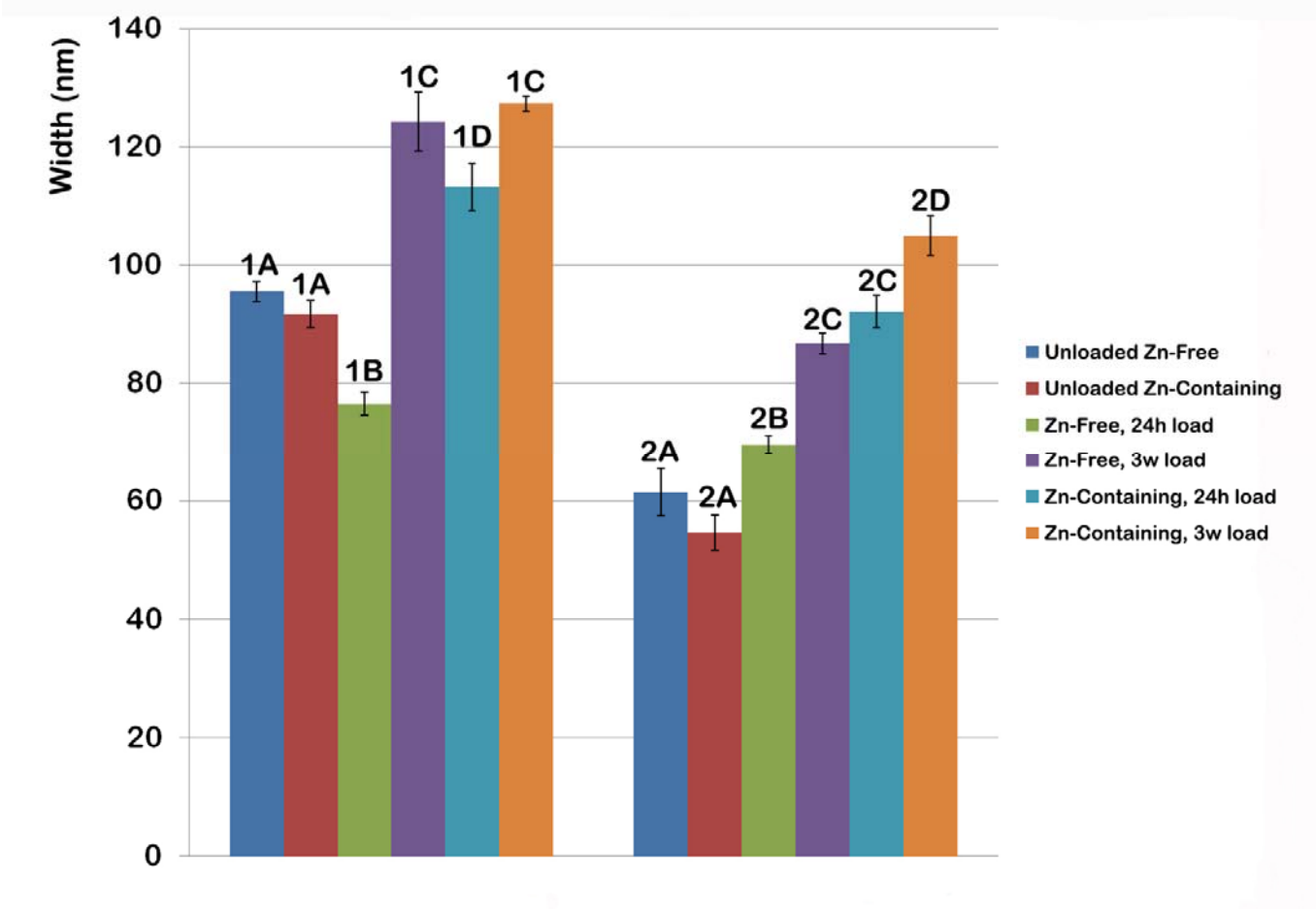

Figure 8. Mean and standard deviation of fibrils width (nm) before amalgam application and after removal of Zn-free or -containing amalgam restorations, unloaded or after 24 hours or 3 weeks of load cycling. Values with identical numbers (between sound dentin and caries-affected dentin) or letters (within sound dentin or caries-affected dentin) indicate no significant differences after Student-Newman-Keuls test ($p>0.05$).

Figure 9 is showing AFM images of caries-affected dentin surface unloaded before amalgam placement, or after load cycled for 3 weeks, with Zn-free or Zn-containing amalgams removal.

Figure 9

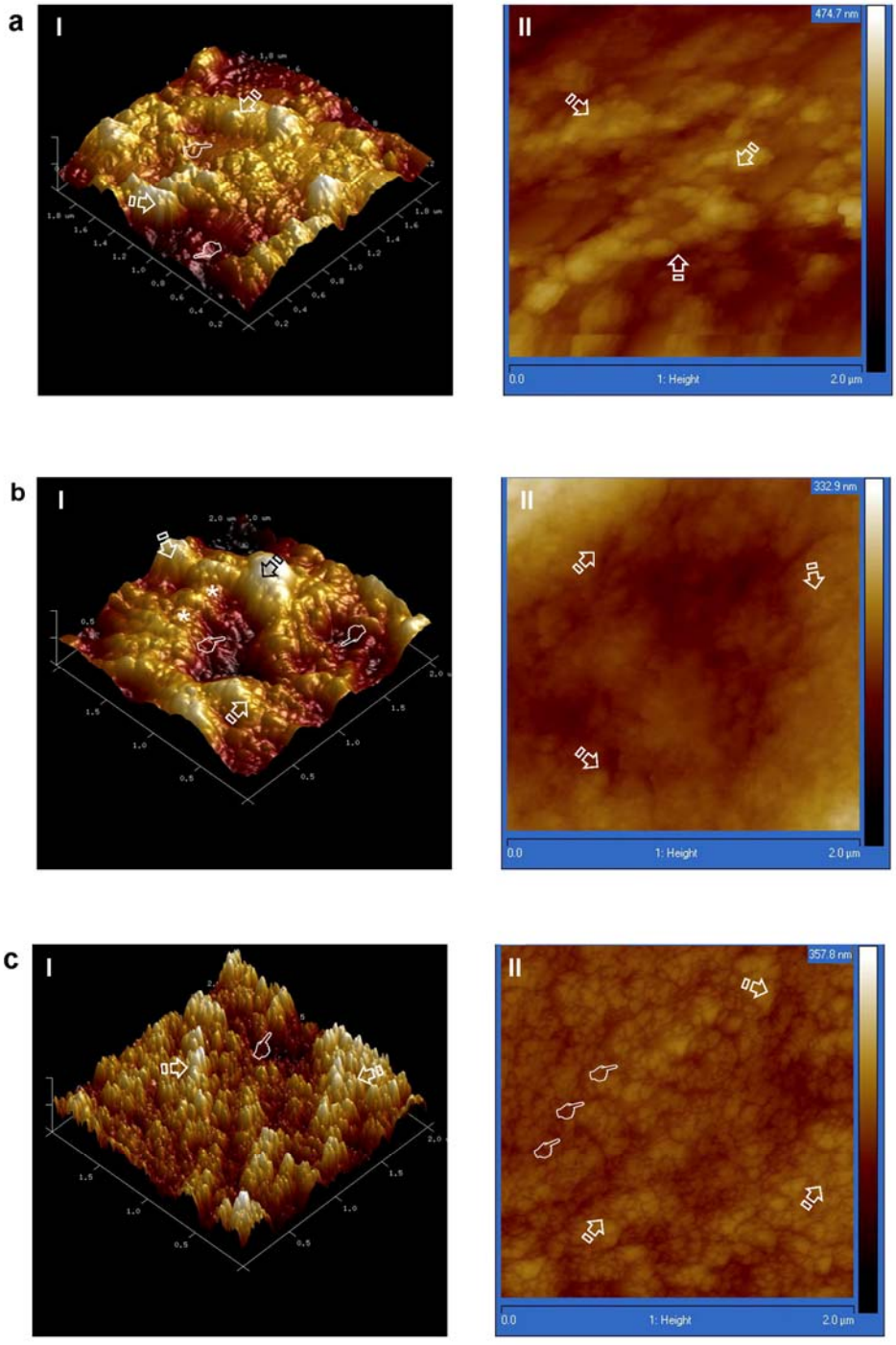

Figure 9. (a): AFM images of caries-affected dentin surface before amalgam placement, unloaded; **aI**, 2 x 2 µm top-view and surface plot image of partially demineralized collagen fibrils (arrows), limiting mineral-depleted areas (pointers); **aII**, AFM phase image (2 x 2 µm) showing the collagen fibrils (arrows). **(b)** AFM images of caries-affected dentin surface restored and load cycled for 3 weeks, after Zn-free

amalgam removal. **bI**, 2 x 2 μm top-view and surface plot image of remineralized collagen fibrils (arrows) which show the staggered pattern of collagen fibrils (asterisks), though limited mineral-depleted areas still exist (pointers); **bII**, AFM phase image (2 x 2 μm) showing the increased bandwidth of the collagen fibrils (arrows). **(c)** AFM images of caries-affected dentin surface restored and load cycled for 3 weeks, after Zn-containing amalgam removal. **cI**, 2 x 2 μm top-view and surface plot image of the totally remineralized collagen fibrils (arrows). The entrance of a tubule may be observed (pointer); **cII**, AFM phase image (2 x 2 μm) showing the wider bandwidth of the collagen fibrils (arrows) and the staggered pattern of collagen fibrils (pointers).

The present research sought to gain insights into the role of different Zn-free or Zn-containing amalgams leading to mechanical recovery and remineralization of partially demineralized dentin in CAD substrata. Nanoindentation is the most commonly applied means of testing the mechanical properties of materials or substrates[47].Young's modulus (E_i) before the placement of amalgam restoration was higher in sound dentin than in caries-affected dentin (CAD) (Table II), as stated by Marshall et al. (2001)[25]. Differences were statistically significant in all study periods, except in the group of restorations performed with Zn-containing amalgam mechanically loaded for 3 w, where CAD attained greater values than SD. At SD surfaces, E_i did not change in any group, except in samples restored with Zn-free amalgam and load cycled for 24 h, which attained a decrease in its modulus of elasticity (Table II). Samples with CAD achieved higher E_i after load cycling for 3 w than the baseline groups, regardless the type of amalgam, but Zn-containing amalgam performed superior.The association between the increase of Young's modulus (E) at the dentin surface and remineralization has been widely demonstrated [48]. Therefore, the null hypothesis that, after load cycling, remineralization is not produced at the SD or CAD surfaces after placement of Zn-free or Zn-containing amalgam restorations, must be partially rejected.

The increase of Young's modulus in CAD samples restored with Zn-containing amalgams became associated to higher values of relative presence on minerals after 3 w of load cycling, in comparison with samples load cycled for 24 h, except in the area of the carbonate peak (CO_3^{2-}) (1070 cm^{-1}) that showed a significant loss of intensity after extended loading (3 w) (Table IVa).These indexes concerned with the maximum relative degree of mineralization [34,35]**.** Intertubular and peritubular mineralization were observed on CAD surfaces restored with Zn-free amalgams after 24 h (Fig 5a) or 3 w (Fig 5b) of load cycling, but extended mechanical loading[49] promoted multiple mineralized formations localized over the total surface of dentin. On the contrary, SD restored with Zn-containing amalgam produced a completely mineralized substratum, where the mineral formations allowed a null display of the tubule entrances (Fig 5c). Nucleation and propagation of hydroxyapatite (HAP) is a multistep process involving both Young's modulus and mineral crystal transition[36]. The univariate intensity map of the Raman shift values of 961 cm^{-1} displayed the highest intensities of the phosphate peak in CAD after both Zn-free and Zn-containing amalgam restorations at 3 w of load cycling (Tables IIIa, IVa) indicating the formation of new mineral in the previous partially demineralized dentin regions. These data were confirmed through our 3D-micro Raman analysis, as the phosphate peak (961 cm^{-1}) increased at the dentin surface (Figs 2c, 4c). Furthermore, this mineralized area was visible in the region at about -5 μm in the X-direction with 5 μm in the Y-direction (Fig 2c), or at the total surface of dentin (Fig 4c). The Raman observations permitted to resolve that on CAD surfaces treated with Zn-containing amalgams the highest peaks at 961 cm^{-1} intensities matched those HAP, the same phase which was observed after Raman spectra of the principal component (Fig 4e). The use of Zn-containing amalgam lead to characteristic nucleated minerals in flake and scale forms surrounded by multiple clumps of precipitated

crystals. This advanced front of mineralization produced a generalized mineral precipitation on the intertubular dentin and occlusion at the entrance of the dentin tubules (Figs 5d, 9·cI).

The Raman phosphate peak at 961cm^{-1} characterizes tetrahedral PO_4 group (P-O bond) within HAP. Monitoring the intensity of this peak has been used to assess the potential increase in phosphate content [36]. Both peaks and areas of phosphate and carbonate groups in CAD also increased in specimens restored with Zn-free amalgams, after 3 w of load cycling. Those minerals crystallized on amorphous nuclei scattered throughout the dentin surface or deposited on a multilayered intertubular dentin and precipitated, visibly (Fig 5b), on the partially demineralized collagen fibers on intertubular dentin (Fig 9·bI) and at the peritubular dentin. Zinc-based salts [phosphorous (P), calcium (Ca), and zinc (Zn)] were detected in the elemental analysis (EDX, spectrum 2), at intertubular dentin. The analysis of μXRD^2 profiles (Fig 6b) permitted to observe an almost complete overlapping, in the range from 24º 2θ to 35º 2θ of traces corresponding to both SD and CAD, except in the 002, 210, 211, and 300 peaks. Those reflections attained greater intensities in CAD than in SD surfaces. The biggest difference was obtained at the 211 reflection (2θ*, 32.303;* centroid peak position θ_{hkl}, -2/1/-2; I, 15293843), where CAD showed ~14x10^4 more counts than SD. Furthermore, 002 reflection, which corresponds to the crystallografic orientation [50] along their long axes [26] was superior in CAD than in SD. At 300 reflexion, both peaks attained approximately similar hight of peaks, though CAD showed ~1.5x10^4 more counts, indicating that crystallites are also orientated along their short axes [26] in, practically, the same proportion. Those discrepancies may also lie in the absence of randomly orientation of nanocrystallites, differences in the grain size and presence of imperfections (stacking faults, twins, dislocations arrays and small-angle boundaries) [50]. The relation between

crystallites orientation, broadening of the μXRD^2 lines, and microstrain requires further research. From 0º 2θ to 24º 2θ, and from 35º 2θ to 100º 2θ, both μXRD^2 profiles followed dissimilar but convergent (<24º 2θ), or divergent (>35º 2θ) plots, but the first indicated lower broadening, *i.e.*, bigger apparent crystallinity in CAD substrata than the latter (SD). Assessment of broadening B_{hkl} peak full-width at half-maximum (FWHM or real crystallinity) through Scherrer-Wilson approximation[26] deserves additional research.

Additionally, extended load cycling [49] showed a reduced symmetry in undistorted trigonal planar carbonate in the crystal lattice, which caused two CO^{3-}_4 peaks (Figs 2e, 4e). This splitting effect into two bands has concerned some changes in this spectral region with carbonate content, ascribed to either growth of a carbonate peak or changes in the phosphate peak in response to the presence of carbonate in the lattice, as the 1,071 cm^{-1} peak is a superposition of carbonate v_1 and phosphate v_3, which can be linearly correlated to the carbonate content of the apatite [51]. Nevertheless, both relative mineral concentration (RMC) and mineral/matrix ratio (MMR) decreased after extended loading [49] in samples restored with Zn-containing amalgams (Table IVa). Those lower presence of minerals comply with lesser modulus of Young (Table II), confirming that the demineralization procedure is functionally intrafibrillar [52].

The principal components that resulted in CAD surfaces restored with Zn-containing amalgams mechanically load cycled for 3 w were phosphorous (P) and calcium (Ca) (Fig 5d·EDX). The absence of Zn^{2+} and Sn^{2+} from the elemental EDX, both performing as a Ca/P growth inhibitor [53] might indicate destabilization of the amorphous state[54], favoring crystallinity at the new nucleated minerals. Chemical mineral crystallinity (Raman-FWHM) express the crystallographic or relative atomic order, since narrower peaks suggest less structural variation in bond distances and

angles[34]. In general, the narrower the spectral peak width is, the higher the degree of mineral crystallinity [35]. This Raman-FWHM increased after observing *data* plotted by the reduced full width and extended height at half maximum of the phosphate band at 961 cm^{-1}, in CAD surfaces restored with Zn-containing amalgams mechanically load cycled for 3 w (Fig 4e), in comparison with *i)* the group load cycled 24 h, and *ii)* sound dentin [49] (Table IVa). μXRD^2 profiles of CAD load cycled 3 w (Fig 6c) showed that the physical broadening of peaks 002 (2θ, 25.900º; 2θ; I, 10977386), 211 (2θ, *32.303;* centroid peak position θ_{hkl}, -2/1/-2; I, 15293843), 222 (2θ, 46978º, centroid peak position θ_{hkl}, -/2/-2; I, 9553174), 213 (2θ, 48.361º, centroid peak position -4/3/-2; I, 2300650), and 004 (2θ, 53.257º; centroid peak position θ_{hkl}, 0/0/-4; I, 4645121) increased when compared with both unloaded SD and CAD substrata (Fig 6a), which in turn suggested the decreased of apparent crystallinity, obtained from diffractometry (XRD-FWHM). The analysis of μXRD^2 profiles comply with the depth profile 2-D XRD Scan frames of SD (Fig 6c, inset a3) and CAD (Fig 6c, inset b3) which showed continuous Debye-Scherrer rings at lower 2θ angles (40.00º). The diffraction rings corresponding to 211, 300 and 202 planes became overlapped and formed a thicker and broad intense ring in both dentin, whereas they were not overlapped when the CAD samples were not submitted to load cycling (Fig 6a, inset a2). The diffraction rings corresponding to 211 and 002 planes formed some bright rings in CAD, and lesser intense in SD (inset a1). Therefore, the lower sharp peaks or peak broadening [50] in the μXRD^2 indicated that the material became more amorphous [55] or with more crystals imperfections in nanocrystallite materias, *i.e,* small crystallite size and lattice distortion [50], after 3 w of load cycling. Furthermore, the present study has also demonstrated that unloaded CAD substrate showed high degrees of apparent crystallinity, *i.e.,* lower

XRD-FWHM or lower degrees of impurity, than the SD substrate, as peaks were sharper in CAD (~16x10^6 counts of intensity) (Fig 6a). Nevertheless, 3 w of load cycling in dentin treated with Zn-containing amalgams achieved an almost overlapping of both SD and CAD assessed with μXRD^2 profiles, indicating quasi similar line broadening of peaks, especially at shifts comprised from 32º to 47º 2θ (Fig 6c).

On the other hand, in samples restored with Zn-containing amalgams mechanically load cycled for 3 w, Raman-FWHM augmented in the group of phosphate (~1.17 fold), but decreased (~0.87 fold) in the group of carbonate (CO_3^{2-}) (1070 cm^{-1}) (Table IV a). This relationship was inverse in the case of sound dentin (increased ~1.53 fold, and decreased ~1.19 fold after 3 w of load cycling, respectively) (Table IV a). Restored teeth with Zn-free amalgams followed the same trend that Zn-containing amalgams (Table IIIa). The formula for stoichiometric HAP is $Ca_{10}(PO_4)_6(OH)_2$. However, in CAD apatite is composed of calcium deficient and carbonate rich apatite crystallites [56], with substitution of CO_3^{2-} for PO_4^{3-} group, leading to a lower Ca/P ratio than that of stoichiometric HAP [26]. Carbonated apatite is a precursor of HAP, as it is unstable. When it is precipitated in the presence of zinc, an exchange between Zn^{2+} and Ca^{2+} may occur forming a substituted apatite compound [57]. The carbonate concentration in calcified tissue provides valuable information and varies with maturity and crystallinity. The presence of B-type carbonate in apatite has been associated with Raman band at ca. 1,070-1,073 cm^{-1}. The carbonate v_1 peaks found at 1,070 cm^{-1}, and its height and area are strongly linked to weight percent carbonate in the apatite [51]. The increment in Raman-crystallinity has been attributed [51,58] to an increase in crystallographic perfection in the apatite unit cell as carbonate substituted for phosphate. On the contrary, the gradient in mineral content (GMC, *i.e.,* carbonate peak/phosphate peak) decreased after 3 w of load cycling in both SD and CAD, in samples restored with

Zn-containing amalgam, and increased in teeth restored with Zn-free amalgams (Tables IIIa, IVa). GMC measures the relative composition differences in the mineral, and clearly determined the average degree of carbonate substitution in apatite [34]. Nevertheless, though GMC diminished after restoring with Zn-containing amalgams mechanically load cycled for 3 w, the obtained minerals were more crystalline (lower Raman-FWHM) and better functionally remineralized (Table II).

Raman analysis also showed that the intensity peak corresponding to normalization (1003 cm^{-1}) increased ~1.50 and 2.07 fold in samples of CAD restored with Zn-containing and Zn-free amalgam, respectively, after 3 w of load cycling*;* on the contrary, normalization decreased in similar conditions when SD was analyzed (Tables IIIb, IVb). An increase in the protein-dependent spectral signal at phenyilalanine preceded the appearance of HAP crystals[36] (Tables IIIb, IVb). Raman spectra of the principal component confirmed this augmentation at the 1003 cm^{-1} band (Figs 2e, 4e). Collagen crosslinking is affected by tissue maturation as well as degree of mineralization, providing information about the structure and molecular interactions of complexes biomolecules [37,59]. Crosslinking of collagen diminished in CAD substrate restored with Zn-containing amalgam after 3 w of load cycling, as pyridinium (1032 cm^{-1}) and ratios 1032/1003, 1660/1690 and 1003/1450 cm^{-1} confirmed this drop after extended mechanical loading (Fig 4e). Those Raman values became linked to a reducible and common crosslinking formation (Table IVb) in association with *i)*: the increment in the relative presence of minerals (Table IVa), *ii)*: the decrease in nanoroughness in comparison with the unloaded specimens (Fig 6), and *iii)*: an increase in the bandwitdth of collagen fibrils (Fig 7). In general, remineralization promoted a decrease in nanoroughness, in comparison to the partially demineralized dentin [60] in CAD substrate. Authors agree that a roughness decrease may be associated to a role of

mineral maturation [61]. Images of specimens remineralized after load cycling for 3 w and removal of Zn-containing amalgam revealed fibrillar structures with significant topographical changes that suggest a preferential organization of mineral within the surface of collagen fibrils, in an intrafibrillar manner [62]. The remineralization procedure made the fibrils to exhibit a growing width of ~ 104 nm (Fig 8), and under higher magnification, the prototypical 67-nm-D-periodicity banding of collagen fibrils [61] was observed. This typical staggered pattern of collagen fibrils (Figs 9·bI, 9·cII) was not visible in the partially demineralized dentin of CAD (Fig 9a), but was evident when this substrate became clearly remineralized (Fig 9c). This finding is consistent with fibrils containing intrafibrillar or extrafibrillar mineral [61,63].

Collagen crosslinking improved mechanical strength and stability of dentin collagen [40], and permitted the growing of minerals within the demineralized dentin, as three-dimensional structures supporting effective mineralization may be created between intrafibrillar collagen molecules via the creation of specific crosslink formation that guide proper mineralization [64]. Furthermore, it could be considered as another efficient biochemical way to block collagen from degradation [37]. When Zn-free amalgams were used in both SD and CAD substrata, and after restoring with Zn-containing amalgam SD samples, crossslinking performed dissimilar (Tables IIIb, IVb) (Figs 1, 2, 3). Nevertheless, AGES-pentosidine (1550 cm^{-1}) increased in the same conditions (Table IVb), even when Zn-free amalgams were used as restorative (Table IIIb) (Fig 2e).The intensity peak of the carboxylic group (COO^-) at 1415cm^{-1} increased ~1.57 and ~1.75 fold in samples of CAD restored with Zn-containing and Zn-free amalgams, respectively, and load cycled for 3 w (Table IVb).This might suggest the formation and further increase of ionic bond with calcium [65]. Band shifts corresponding to lipids (1440 and 1465 cm^{-1}) augmented (~1.46 and 1.61 fold, respectively) in samples

of CAD restored with Zn-containing and load cycled for 3 w (Table IVb). Similar trend was followed when Zn-free amalgams were used in the same conditions, with raises of ~1.80 and 1.56 fold, respectively (Table IIIb).Those spectral changes observed in the lipid bands confirm the presence of tissue healing and maturation [43].

Peaks concerning nature and secondary structure of collagen, in samples of CAD restored with Zn-containingor Zn-free amalgams and load cycled for 3 w, increased in all components and ratios, except in A-III/CH_2 (Table IVc), as A-III (Table IVc) (Figs 2e, 4e) augmented in similar conditions.These ratios and indexes are expected to increase when mineralization occurs[33], preceding the appearance of phosphate stretching peak at 960 cm^{-1} (Figs 2c, 4c); this purports that nucleation is a multistep process involving both protein and mineral transition, suggesting a temporally synchronized process [66]. Dissimilar performance was attained when SD was analyzed in the same conditions (Tables IIIc, IVc). RatioA-I/AGEs-Pentosidine, indicative of the glycation reaction *vs* collagen scaffolding [45] increased in samples of CAD restored with Zn-containing or Zn-free amalgams and load cycled for 3 w. Glycation promoted formation of cross-links between molecules, causing an increase in the area of the extracellular matrix, resulting in increased stiffness [67]. Through scaffolding, local environmental conditions for guiding and assisting the generation of natural extracellular matrix and mineral deposition are provided, and so mechanical integrity and functionality [68]. Band shifts corresponding to α-helices dropped (~5. 53 fold) in samples of CAD restored with Zn-containing and load cycled for 3 w (Table IVc) (Fig 4e), but augmented ~1.80 fold when Zn-free amalgams were used in similar conditions (Table IIIc) (Fig 2e). The1340 cm^{-1} tracing line exhibited a very low level of noise of fluctuation (Fig 4e). Interestingly, this orientation-sensitive signal decreased when mineralization was allowed to proceed [36], corroborated by the high Young's modulus

values that obtained (Table II). It is noteworthy that the protein-dependent spectral signal at α-helices (1340 cm^{-1}) in samples of CAD restored with Zn-containing and load cycled for 3 w shows a peak of 0.94 (the lowest) and some of the highest peaks in both 960 cm^{-1} (phosphate) (66.05) (Fig 4c) and 1070 cm^{-1} (carbonate) (13.89) (Table IVa). Therefore, it can be assumed that this decrease (α-helices) precedes the appearance of HAP.

These are, to the best of our knowledge, the only available results from remineralization experiments on partially mineral-depleted substratum in caries-affected dentin surfaces restored with Zn-free *vs* -containing amalgams submitted to short (24 h) or extended (3 w) stimuli of load cycling. These outcomes are important, because they provide information on structure and mechanical, morphological physical and chemical changes produced at micro and nano-scale at demineralized dentin below Zn-containing amalgams; however, additional correlation analyses of properties of the whole new surface are still needed. In this line, it is recommended to determine the grain size and lattice microstrain accordingly determined by measuring the deviation of line profile from perfect crystal diffraction. To evaluate the viscoelastic changes of the dentin surface in contact with Zn-containing amalgams, produced at nano-scale, is still needed. Hence, improving the dissipation of energy within the restorative-dentin interface becomes imperative for enhancing therapy and expanding the lifetime of dental restorations. Further work is now required to determine the mechanism by which load and thermal cycling prevent mechanical and thermal induced changes in dentin mineralization and dentin strength.

ACKNOWLEDGMENTS.

This work was supported by grants MINECO/FEDER MAT2014-52036-P and FIS2013-41821-R. The authors have no financial affiliation or involvement with any commercial organisation with direct financial interest in the materials discussed in this manuscript. Any other potential conflict of interest is disclosed.

REFERENCES

[1.] X. Yuan, W. Jinglei, W. Haoming, L. Hanqin, D. Ning, S. Lei, L. Sontaoi, L. ianwei, X. Yang, L.Wei, M. Xiumei, and Z. Qiang, Tissue Eng. Pt.C-Meth. **19**, 925 (2013). doi:10.1089/ten.tec.2012.0328.

[2.] Z. Xie, M. Swain, P.Munroe, and M. Hoffman, Biomaterials **29**, 2697 (2008). doi: 10.1016/j.biomaterials.2008.02.022.

[3.] Y. Wang, P. Spencer, and M.P. Walker, J. Biomed. Mater. Res. A **81**, 279 (2007). doi:10.1002/jbm.a.30981.

[4.] L. Zheng, J.F. Hilton, S. Habelitz, S.J. Marshall, and G.W. Marshall, Eur. J. Oral Sci. **111**, 243 (2003). doi: 10.1034/j.1600-0722.2003.00038.x.

[5.] M. Yoshiyama, F.R. Tay, Y. Torii, Y. Nishitani, J. Doi, K. Itou, B. Ciucchi, and D.H. Pashley, Am J. Dent. **16**, 47 (2003).

[6.] T.F. Watson, A.R. Atmeh, S. Sajini, R.J. Cook, and F. Festy, Dent. Mater. **30**, 50 (2014). doi: 10.1016/j.dental.2013.08.202.

[7.] S.K. Makhija, V.V. Gordan, G.H. Gilbert, M.S. Litaker, D.B. Rindal, D.J. Pihlstrom, and V. Qvist, J. Am. Dent. Assoc. **142**, 622 (2011).

[8.] K. Lyons; Ministry of Health, N. Z. Dent. J. **99**, 10 (2003).

[9.] M.G. Rasines Alcaraz, A.Veitz-Keenan, P. Sahrmann, P.R. Schmidlin, D. Davis, Z. Iheozor-Ejiofor, Cochrane Database Syst. Rev. **31,** 3 (2014). doi: 10.1002/14651858.CD005620.pub2.

[10.] ADA (American Dental Association) (2013). http://www.ada.org/1741.aspx. Statement on dental amalgam.

[11.]FDA (US Food and Drug Administration) (2013). http://www.fda.gov/MedicalDevices/ProductsandMedicalProcedures/DentalProducts/Dental Amalgam/ucm171094.htm. About dental amalgam fillings.

[12.] FDA (US Food and Drug Administration), Fed. Regist. **74**, 38686 (2009). Dental devices:classification of dental amalgam, reclassification of dental mercury, designation of special controls for dental amalgam, mercury, and amalgam alloy.

[13.] K.G. Homme, J.K. Kern, B.E. Haley, D.A. Geier, P.G. King, L.K. Sykes, and M.R. Geier, Biometals **27**, 19 (2014). doi: 10.1007/s10534-013-9700-9.

[14.] J. Mutter, J. Naumann, and C. Guethin, Crit. Rev. Toxicol. **37**, 537 (2007). doi: 10.1080/10408440701385770.

[15.] G. Alexander, M.S. Hopcraft, M.J. Tyas, and R.H.Wong, Aust. Dent. J. **59**, 408 (2014). doi: 10.1111/adj.12209.

[16.] N.J. Opdam, E.M. Bronkhorst, B.A. Loomans, and M.C. Huysmans, J. Dent. Res. **89**, 1063 (2010). doi:10.1177/0022034510376071.

[17.] P. Spencer, Q. Ye, A. Misra, S.E.P. Goncalves, and S.J. Laurence, J. Dent. Res. **93**, 1243 (2014). doi: 10.1177/0022034514550039.

[18.] K. Anusavice. Phillips' Science of Dental Materials, 11th ed. (Saunders Publishing Co., Elsevier, St. Louis,2003), pp.832.

[19.] J.H. Watkins, H. Nakajima, K. Hanaoka, L. Zhao, T. Iwamoto, and T. Okabe, Dent. Mater. **11**, 24 (1995).

[20.] J.D. Scholtanus, W. Van der Hoorn, M. Özcan, M.C**.** Huysmans, F.J. Roeters, C.J. Kleverlaan, and A.J. Feilzer, Am. J. Dent. **26**, 185 (2013).

[21.] S.J. Marshall, G.W. Marshall Jr, and H. Letzel, Dent. Mater. **8**, 162 (1992).

[22.]M. Toledano, F.S. Aguilera, E. Osorio, I. Cabello, M. Toledano-Osorio, and R. Osorio, J. Mech. Behav. Biomed. Mater.**47,** 65 (2015) doi:10.1016/j.jmbbm.2015.03.012.

[23.] M. Toledano, F.S. Aguilera, E. Osorio, I. Cabello, M. Toledano-Osorio, and R.Osorio, Bio*interphase*s (2015). In press.

[24.] L.E. Bertassoni, S. Habelitz, J.H. Kinney, S.J. Marshall, and G.W. Marshall Jr., Caries Res. **43**, 70 (2009). doi: 10.1159/000201593.

[25.] G.W. Marshall, S. Habelitz, R. Gallagher, M. Balooch, G. Balooch, S.J. Marshall, J. Dent. Res. **80,** 1768 (2001). doi: 10.1177/00220345010800081701.

[26.] J. Xue, A.V. Zavgorodniy, B.J. Kennedy, M.V. Swain, and W. Li, J. Microsc. **251**, 144 (2013). doi: 10.1111/jmi.12053.

[27.] T. Kokubo, H. Takadama H. Biomaterials **27**, 2907 (2006). doi:10.1016/j.biomaterials.2006.01.017.

[28.] L. Han, A.J. Grodzinsky, and C. Ortiz, Annu. Rev. Mater. Res. **41**, 133 (2011). doi: 10.1146/annurev-matsci-062910-100431.

[29.] W.C. Oliver, and G.M. Pharr, J. Mater. Res. **7,** 1564 (1992). doi: 10.1557/JMR.1992.1564.

[30.] S. Habelitz, M. Balooch, S.J. Marshall, G. Balooch, G.W. and Marshall Jr., J. Struct. Biol. **138**, 227 (2002). doi:10.1016/S1047-8477(02)00029-1.

[31.] K. Takeyasu, H. Omote, S. Nettikadan, F. Tokumasu, A. Iwamoto-Kihara, and M. Futai, FEBS Letters **392,** 110 (1996). doi:10.1016/0014-5793(96)00796-X.

[32.] A. Almahdy, F.C. Downey, S. Sauro, R.J. Cook, M. Sherriff, D. Richards, T.F. Watson, A. Banerjee, and F. Festy, Caries Res. **46**, 432 (2012). doi: 10.1159/000339487.

[33.] M. Toledano, F.S. Aguilera, I. Cabello, and R. Osorio, Biomech. Model. Mechan. **13**, 1289. (2014c). doi: 10.1007/s10237-014-0573-9.

[34.] A.G. Schwartz, J.D. Pasteris, G.M. Genin, T.L. Daulton, S. Thomopoulos S. PLoS One **7**, e48630 (2012). doi: 10.1371/journal.pone.0048630.

[35.] K. Karan, X. Yao, C. Xu, and Y. Wang, Dent. Mater. **25**, 1205 (2009). doi: 10.1016/j.dental.2009.04.006.

[36.] C. Wang, Y. Wang, N.T. Huffman, C. Cui, X. Yao, S. Midura, R.J. Midura, and J.P. Gorski, J. Biol. Chem. **284**, 7100 (2009). doi: 10.1074/jbc.M805898200.

[37.] C. Xu and Y. Wang, J. Biomed. Mater. Res. B Appl. Biomater. **96**, 242 (2011). doi: 10.1002/jbm.b.31759.

[38.] U. Daood, K. Iqbal, L.I. Nitisusanta, and A.S. Fawzy AS, J. Biomed. Mater. Res. A **101**, 1846 (2013). doi:10.1002/jbm.a.34482.

[39.] M. Jastrzebska, R. Wrzalik, A. Kocot, J. Zalewska-Rejdak, and B. Cwalina, J. Biomater. Sci. Polym. Ed. **14**, 185 (2003).

[40.] C. Xu and Y. Wang, J. Adhes. Dent. **14**, 11 (2012). doi: 10.3290/j.jad.a21494.

[41.] D.R. Sell and V.M. Monnier, J. Biol. Chem. 264, 21597 (1989).

[42.] M.A. Strehle, P. Rösch, R. Petry, A. Hauck, R. Thull, W. Kiefer, and J. Popp, Phys. Chem. Chem. Phys. **6**, 5232 (2004). doi: 10.1039/B406524G.

[43.] G. Penel, C. Delfosse, M. Descamps, and G. Leroy, Bone **36**, 893. (2005). doi: 10.1016/j.bone.2005.02.012

[44.] J.W. Ager, R.K. Nalla, G. Balooch, G. Kim, M. Pugach, S. Habelitz, G.W. Marshall, J.H. Kinney, and R.O. Ritchie, J. Bone Miner. Res. **21**, 1879 (2006). doi: 10.1359/jbmr.060816.

[45.] H. Salehi, E. Terrer, I. Panayotov, B. Levallois, B. Jacquot, H. Tassery, and F. Cuisinier, J. Biophotonics **6**, 765 (2013). doi: 10.1002/jbio.201200095.

[46.] International Centre for Diffraction Data (2005) Powder Diffration File 09-0432.

[47.] B. Poon, D. Rittel, and G. Ravichandran. Int. J. Solids Struct. **45**, 6018 (2008). doi:10.1016/j.ijsolstr.2008.07.021.

[48.] L.E. Bertassoni, S. Habelitz, S.J. Marshall, and G.W. Marshall, J. Biomech. **44**, 176 (2011). doi: 10.1016/j.jbiomech.2010.09.005.

[49.] M. Toledano, F.S. Aguilera, S. Sauro, I. Cabello, E. Osorio, and R. Osorio, Dent. Mater. **30**, e169. (2014). doi: 10.1016/j.dental.2014.02.009.

[50.] Z. Zhang, F. Zhou, and E.J. Lavernia, J. Metall. Mater. Trans. **34**, 1349 (2003).

[51.] A. Awonusi, M.D. Morris, and M.M. Tecklenburg, Calcif. Tissue Int. **81**, 46 (2007). doi: 10.1007/00223-007-9034-0.

[52.] J.H. Kinney, S. Habelitz, S.J. Marshall, and G.W. Marshall, J. Dent. Res. **82,** 957(2003). doi: 10.1177/154405910308201204.

[53.] A. Hoppe, N.S. Güldal, and A.R. Boccaccini, Biomaterials **32,** 2757 (2011). doi: 10.1016/j.biomaterials.2011.01.004.

[54.] F. Barrére, P. Layrolle, C.A. van Blitterswijk, and K. de Groot, Bone **25**, 107S (1999). doi:10.1016/S8756-3282(99)00145-3.

[55.] A. Moshaverinia, S. Ansari, M. Moshaverinia, N. Roohpour, J.A. Darr, and I. Rehman, Acta Biomater **4**, 432 (2008). doi:10.1016/j.actbio.2007.07.011.

[56.] M.T. Fulmer, and P.W. Brown, J. Biomed. Mater. Res. **27**, 1095 (1993). doi: 10.1002/jbm.820270815.

[57.] R. Osorio, E. Osorio, I. Cabello, and M. Toledano, Caries Res. **48**, 276 (2014). doi:10.1159/000356873.

[58.] A. Krajewski, M. Mazzocchi, P.L. Buldini, A. Ravaglioli, A. Tinti, P. Taddei, and C. Fagnano, J. Molec. Struct. **744**, 221 (2005). doi:10.1016/j.molstruc.2004.10.044.

[59.] M. Saito, K. Fujii, and K. Marumo, Calcif. Tissue Int. **79**, 160 (2006).doi: 10.1007/s00223-006-0035-1.

[60.] M. Toledano, E. Osorio, I. Cabello, and R. Osorio, J. Dent. **42**, 384 (2014). doi: 10.1016/j.jdent.2014.01.012.

[61.] K.M. Zurick, C. Qin, and M.T. Bernards, J. Biomed. Mater. Res. Part A **101**, 1571 (2013). doi: 10.1002/jbm.a.34462.

[62.] D.S. Kim, J. Kim, K.K. Choi, and S.Y. Kim, J. Dent. **39**, 855 (2011). doi: 10.1016/j.jdent.2011.09.010.

[63.] L.E. Bertassoni, S. Habelitz, M. Pugach, P.C. Soares, S.J. Marshall, and G.W. Marshall Jr, Scanning **32**, 312 (2010). doi: 10.1002/sca.20199.

[64.]M. Saito and K. Marumo, Front. Endocrinol. **4**, 72 (2013). doi: 10.3389/fendo.2013.00072.

[65.] E. Coutinho, Y. Yoshida, S. Inoue, R. Fukuda, J. Snauwaert, Y. Nakayama, J. De Munck, P. Lambrechts, K. Suzuki, and B. Van Meerbeek, J. Dent. Res. **86**, 656. (2007). doi: 10.1177/154405910708600714.

[66.]Y. Wang, and X. Yao, Dent. Mater. **26**, 433 (2010). doi: 10.1016/j.dental.2010.01.002.

[67.] A. Goldin, J.A. Beckman, A.M. Schmidt, and M.A. Creager, Circulation **8**, 114. (2006).doi:10.1161/CIRCULATIONAHA.106.621854.

[68.] L. Zhang, Y. Morsi, Y. Wang, L. Yubao, and S. Ramakrishna, Jpn. Dent. Sci. Rev. **49**, 14 (2013). doi:10.1016/j.jdsr.2012.09.001.

Figure captions

Figure 1. RAMAN analysis of sound dentin after removal of load cycled Zn-free amalgam restoration. 3D micro-Raman map of 961 cm^{-1} intensities at the dentin surface when load cycling was applied for 24 h **(a)** or 3 w **(c)**. At the 3D micro-Raman, blue represents the lowest peak intensity, while the red represents the highest. K-means clustering (KMC) map of the Raman profile of the same samples, when load cycling was applied for 24 h **(b)** or 3 w **(d)**. **(e)** Raman spectra of the principal component.

Figure 2. RAMAN analysis of caries-affected dentin after removal of load cycled Zn-free amalgam restoration. 3D micro-Raman map of 961 cm^{-1} intensities at the dentin surface when load cycling was applied for 24 h **(a)** or 3 w **(c)**. At the 3D micro-Raman, blue represents the lowest peak intensity, while the red represents the highest. K-means clustering (KMC) map of the Raman profile of the same samples, when load cycling was applied for 24 h **(b)** or 3 w **(d)**. **(e)** Raman spectra of the principal component.

Figure 3. RAMAN analysis of sound dentin after removal of load cycled Zn-containing amalgam restoration. 3D micro-Raman map of 961 cm^{-1} intensities at the dentin surface when load cycling was applied for 24 h **(a)** or 3 w **(c)**. At the 3D micro-Raman, blue represents the lowest peak intensity, while the red represents the highest. K-means clustering (KMC) map of the Raman profile of the same samples, when load cycling was applied for 24 h **(b)** or 3 w **(d)**. **(e)** Raman spectra of the principal component.

Figure 4. RAMAN analysis of caries-affected dentin after removal of load cycled Zn-containing amalgam restoration. 3D micro-Raman map of 961 cm^{-1} intensities at the dentin surface when load cycling was applied for 24 h **(a)** or 3 w **(c)**. At the 3D micro-Raman, blue represents the lowest peak intensity, while the red represents the highest. K-means clustering (KMC) map of the Raman profile of the same samples, when load

cycling was applied for 24 h **(b)** or 3 w **(d)**. **(e)** Raman spectra of the principal component.

Figure 5. (a): FESEM image and EDX spectrum of caries-affected dentin after removal of Zn-free amalgam restoration, and 24 h of load cycling. Peritubular (PD) and intertubular (ID) dentin were strongly mineralized. A consistent and continuous layer of mineral was observed covering the intertubular dentin (asterisk). Mineralized collagen fibrils were not noticeable below this coat of new crystals. Some crystals or mineral deposits were occasionally encountered on both intertubular and peritubular dentin (arrows). Tubules appeared mineral free with a clear ring of peritubular dentin (double arrow) and a robust peritubular dentin wall (pointer). Ep1 is an EDX spectrum indicating presence of phosphorous (P), calcium (Ca) and tin (Sn). (**b):** FESEM image and EDX spectrum of caries-affected dentin (CAD) after removal of Zn-free amalgam restoration, and 3 w of load cycling. A compact mineralized layer appeared covering the whole intertubular dentin (ID). At peritubular dentin (PD), mineral formed a lip around each tubule lumen detected.-Collagen fibers were clearly observed at peritubular dentin, some of them partially (arrow), or totally remineralized (pointer), permitting to observe the presence of mineral crystals embedded in a remnant collagen scaffold-like structure. Multiple mineralized formations scattered throughout the total surface of dentin (double arrow), but allowing the visual observation of tubule walls. Some non-sealed tubules turned up partially mineral filled (asterisk). Collagen fibrils appeared longitudinally mineralized, rounding the entrance of tubules. Ep2 is an EDX spectrum, corresponding to intertubular dentin location, indicating presence of phosphate (P), calcium (Ca) and tin (Sn), among the principal components. **(c):** FESEM image and EDX spectrum of sound dentin after removal of Zn-containing amalgam restoration, and 24 h of load cycling. Tubules appeared totally mineral-occupied with a complete hermetic sealing

(arrows). Crystals precipitated in small and inter-connected knob-like formations, at intertubular dentin (ID), and smaller at intratubular dentin (pointer). Zinc-based salts [phosphorous (P), calcium (Ca), and zinc (Zn)] were detected in the elemental analysis (EDX, spectrum 3). **(d):** FESEM image and EDX spectrum of caries-affected dentin (CAD) after removal of Zn-containing amalgam restoration and 3 w of load cycling. A consistent and continuous layer of mineral was observed covering the intertubular dentin (asterisk), precipitating in a dense network of multilayered crystals on the dentin surface. These crystal formations did not allow to see the subjacent collagen fibers, and covered partially (arrow) or totally (double arrow) the entrance of tubules. Some terminal knob-like mineral structures were exhibited on the dentin surface, occupying spaces among the mineral scales. Most of the tubules appeared mineral-occupied without hermetic sealing (pointer), in some cases. Ep4 is an EDX spectrum, corresponding to intertubular dentin location, indicating presence of phosphate (P), and calcium (Ca).

Figure 6. **(a)** Refined μXRD^2 profiles of unloaded sound and caries-affected dentin. The corresponding Debye-Scherrer rings are shown in inset a1 (sound dentin) and b1 (caries-affected dentin). **(b)** Refined μXRD^2 profiles of sound and caries-affected dentin after removal of Zn-free amalgam and three weeks of load cycling. The corresponding Debye-Scherrer rings are shown in inset a2 (sound dentin) and b2 (caries-affected dentin). **(c)** Refined μXRD^2 profiles of sound and caries-affected dentin after removal of Zn-containing amalgam and three weeks of load cycling. The corresponding Debye-Scherrer rings are shown in inset a3 (sound dentin) and b3 (caries-affected dentin).

Figure 7. Mean and standard deviation of nanoroughness Sra (nm) measured on sound and caries-affected dentin surfaces, after removal of Zn-free or -containing amalgam restorations, unloaded or after 24 hours or 3 weeks of load cycling. Identical letters

(lower case, sound dentin; capital, caries-affected dentin) indicate no significant differences after Student-Newman-Keuls test ($p>0.05$). *indicates significant differences between sound dentin and caries-affected dentin, within the same group.

Figure 8. Mean and standard deviation of fibrils width (nm) before amalgam application and after removal of Zn-free or -containing amalgam restorations, unloaded or after 24 hours or 3 weeks of load cycling. Values with identical numbers (between sound dentin and caries-affected dentin) or letters (within sound dentin or caries-affected dentin) indicate no significant differences after Student-Newman-Keuls test ($p>0.05$).

Figure 9. (a): AFM images of caries-affected dentin surface before amalgam placement, unloaded; **aI**, 2 x 2 μm top-view and surface plot image of partially demineralized collagen fibrils (arrows), limiting mineral-depleted areas (pointers); **aII**, AFM phase image (2 x 2 μm) showing the collagen fibrils (arrows). **(b)** AFM images of caries-affected dentin surface restored and load cycled for 3 weeks, after Zn-free amalgam removal. **bI**, 2 x 2 μm top-view and surface plot image of remineralized collagen fibrils (arrows) which show the staggered pattern of collagen fibrils (asterisks), though limited mineral-depleted areas still exist (pointers); **bII**, AFM phase image (2 x 2 μm) showing the increased bandwidth of the collagen fibrils (arrows). **(c)** AFM images of caries-affected dentin surface restored and load cycled for 3 weeks, after Zn-containing amalgam removal. **cI**, 2 x 2 μm top-view and surface plot image of the totally remineralized collagen fibrils (arrows). The entrance of a tubule may be observed (pointer); **cII**, AFM phase image (2 x 2 μm) showing the wider bandwidth of the collagen fibrils (arrows) and the staggered pattern of collagen fibrils (pointers).